



TECHNISCHE
UNIVERSITÄT
WIEN
Vienna University of Technology

Unterschrift Betreuer

DIPLOMARBEIT

Magnetic Field Freezing

Ausgeführt am Institut für Festkörperphysik
der Technischen Universität Wien

unter der Anleitung von

Privatdoz. Dipl.-Ing. Dr.techn. Dieter Suess

durch

Olivia Muthsam, 1026161

Dr.E.Schrödingerstraße 6, 2000 Stockerau

10. September 2016

Unterschrift Studentin

Zusammenfassung

Simulationen von isotropen Permanentmagneten verlangen die Modellierung von vektorieller Hysterese. Diese Hystereseemodelle sind oft sehr kompliziert und benötigen meist großen rechnerischen Aufwand und Messungen am Material um die benötigten Materialdaten abzuleiten. Ziel dieser Arbeit ist es ein einfacheres Vektor-Hysterese Modell, das sogenannte Freezing Modell, zu untersuchen und den benötigten Parameter, das Freezing Feld H_{freeze} , für verschiedene Geometrien und unterschiedliche Materialien zu finden.

Für die Simulationen des isotropen Magneten wurde zur Lösung von magneto-statischen Maxwell Gleichungen eine Koppelung von FEM und BEM verwendet.[1] Als spezielle Implementierung wurde in dieser Arbeit FEMME genutzt, in dessen Code sich die Freezing Bedingung leicht einfügen lässt. Das Freezing Modell wurde mit einem Hysterese-freiem anisotropen Magnetmodell verglichen und die Unterschiede analysiert. Mit Hilfe eines Computereperiments, das auf einem Stoner-Wohlfarth Modell basiert, konnten Grenzen für das Freezing Feld theoretisch bestimmt werden. Messungen mit echten Magneten, produziert von der Magnetfabrik Bonn, wurden anschließend mit den FEMME Simulationen verglichen.

Es wurde herausgefunden, dass das Freezing Feld höher ist, als es aufgrund eines Stoner-Wohlfarth Modells erwartet wird. Außerdem ist H_{freeze} sehr stark abhängig von der Wahl der Remanenzmagnetisierung in den Simulationen und bleibt somit in gewisser Weise ein Fitting Parameter.

In der folgenden Arbeit werden die Grundlagen der Simulationen von isotropen Permanentmagneten erklärt und verschiedene Hystereseemodelle aufgeführt. Anschließend wird das Freezing Modell genauer untersucht und das Freezing Feld H_{freeze} gesucht.

Abstract

Simulations of isotropic permanent magnets require modeling of vectorial hysteresis. These hysteresis models are often complicated and have high computational effort and need measurements on the material to identify various needed material parameters. The goal of this work is to analyze a simpler vector hysteresis model, the so-called freezing model, and to determine the needed freezing parameter H_{freeze} for different geometries and various materials.

To simulate isotropic magnets magnetostatic Maxwell equations are solved with the help of FEM-BEM coupling.[1] The implementation that is used in this work is FEMME. The freezing condition can easily be implemented additionally to already existing simulations of isotropic magnets. The freezing model was compared to a hysteresis free, anisotropic magnet model and differences were analyzed. With the help of a computer experiment, which is based on a Stoner-Wohlfarth model, boundaries of the freezing field were theoretically determined. Measurements of real magnets, produced by Magnetfabrik Bonn were compared afterwards with FEMME simulations.

The obtained freezing field was higher than expected by a Stoner-Wohlfarth model. Additionally, H_{freeze} heavily depends of the choice of the remanent magnetization in the simulations and thus somehow is a fitting parameter.

In the following work, basics of isotropic permanent magnets will be explained and different hysteresis models will be presented. Afterwards the freezing model will be explained more precisely and the freezing field H_{freeze} will be determined.

Danksagung

An dieser Stelle möchte ich zuerst meinem Betreuer Privatdoz.Dipl.-Ing.Dr.techn. Dieter Suess danken, der meine Diplomarbeit betreut hat und mich während der ganzen Zeit umfangreich unterstützt hat. Dank seiner Expertise und der konstruktiven Kritik habe ich fachlich sehr viel dazugelernt. Vielen Dank auch für die Organisation der finanziellen Unterstützung meiner Arbeit.

Weiters gilt mein besonderer Dank meinem Ko-Betreuer Projektass.Dipl.-Ing.Dr.techn. Florian Bruckner, der sich immer Zeit für mich genommen und mir stets weitergeholfen hat. Durch seine geduldigen Erklärungen wurde mein Verständnis für das Thema vertieft und ich wurde jedes Mal aufs Neue motiviert.

Herzlich danken möchte ich auch der gesamten Arbeitsgruppe, die dafür gesorgt hat, dass ich mich im Team sehr wohl gefühlt habe und während der Arbeit auch viel Spaß hatte. Speziell hervorheben möchte ich Gregor Wautischer, der mich in die Arbeitsgruppe geholt hat und mir besonders am Anfang meiner Diplomarbeit viel Hilfestellung geleistet hat.

Vielen Dank auch an die Mitarbeiter von Infineon und der Magnetfabrik Bonn, die bei den Telefonkonferenzen durch Diskussionen neue Fragen angeregt haben und uns die Messdaten zur Verfügung gestellt haben.

Ein großer Dank gebührt meiner Familie, die mich immer tatkräftig unterstützt und an mich geglaubt hat. Besonders möchte ich meinen Eltern danken, dass sie mir das Studium ermöglicht und mich bei meinen Entscheidungen unterstützt haben.

Ganz besonders danken möchte ich auch meinem Freund Gregor Gantner, der immer ein offenes Ohr für mich hatte und selbst in der stressigsten Zeit mein Ruhepol war.

Schließlich möchte ich noch meinen Studienkollegen danken, die meine Studienzeit unvergesslich gemacht haben. Mein spezieller Dank gilt Lena Bauer, ohne die das Studium nur halb so viel Spaß gemacht hätte und die immer für mich da war.

Contents

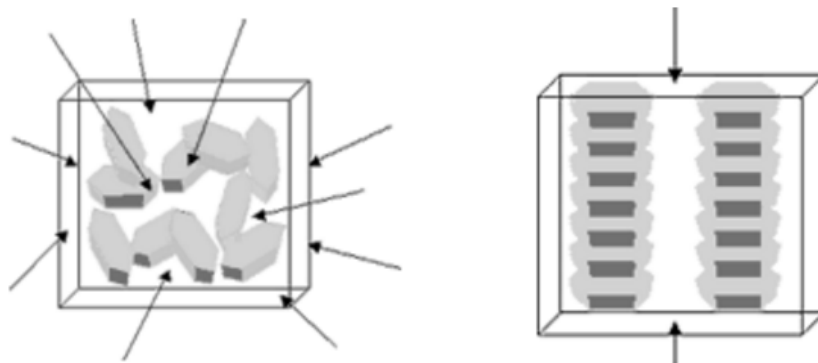
1	Introduction	7
2	Modelling Magnetic Materials	10
2.1	Hysteresis	10
2.2	Soft Magnetic Materials	12
2.2.1	General Differential Formulation of Maxwell's Equations	13
2.2.2	Magnetostatic Maxwell Equations	16
2.2.3	Reduced Scalar Potential Formulation for Soft Magnets	16
2.2.4	Total Scalar Potential Formulation for Soft Magnets	17
2.2.5	Solving Maxwell's Equations	18
2.2.6	Integral Formulation of Maxwell's Equations	19
2.2.7	Method of Moments	21
2.3	Hard Magnetic Materials	24
2.3.1	Maxwell's Equations for Hard Magnets	25
2.3.2	Scalar Preisach Models	25
2.3.3	Vector Preisach Models	27
2.3.4	Stoner - Wohlfarth model	28
2.3.5	Freezing Model	32
3	Comparing Freezing and Anisotropy	35
3.1	Choice of Parameters	35
3.2	Deviation between Freezing and Anisotropy	39
3.2.1	Deviation Measure	40
3.2.2	Visualization of Deviation	41
4	Computer Experiment to Determine H_{freeze}	43
4.1	Stoner - Wohlfarth Model: Setting	43
4.2	Material Parameter	46
4.3	Results	47
4.4	Extended Stoner - Wohlfarth model: Computing H_k and H_c	49
5	Comparing Measurement and Simulation	51
5.1	Measurement	51
5.2	Comparison	53
5.2.1	Simulations	53
5.2.2	Measurement	54
5.2.3	Measurement with Negative Part vs. Non-freezing Simulation	56

5.2.4	Measurement without Negative Part vs. Freezing Simulation	56
5.2.5	Results with Fitted Parameters - All Materials	57
5.2.6	Non-reproducible Measurement Data	59
5.2.7	Results - Data Sheet All Materials	60
5.3	Conclusion	62
6	Discussion and Outlook	63
6.1	Main Results	63
6.2	Future Development	64

1 Introduction

The accurate simulation of permanent magnets is necessary since they are used for many applications, for example in electric motors, hard disks, generators, magnetic amplifiers and magnetic sensors. There are two types of permanent magnets, isotropic and anisotropic magnets which have to be simulated differently, since they have different characteristics.

Anisotropic magnets are characterized by the fact that they have a preferred direction of magnetization (see Figure 1(b)). This is because a magnetic field is applied during the production process, which orientates the magnetic grains into the direction of the applied field.[2] The direction in which the magnet can be magnetized best is called easy axis. The easy axis is the direction inside the crystal in which the smallest external field has to be applied to reach saturation magnetization. The orientation of the easy axis remains even if the applied field is turned off. Even if a high external field is applied after the production process, it does not change the fixed crystallites. Within the whole magnet a homogeneous intrinsic anisotropic material law can be defined.



(a) Crystal arrangement of isotropic magnet
(b) Crystal arrangement of anisotropic magnet

Figure 1: Difference between crystal arrangements of isotropic and anisotropic magnet. While the crystal arrangement of the isotropic magnet is random and the magnet thus can be magnetized in all directions alike, the crystals of an anisotropic magnet are arranged unidirectional along a prescribed axis, resulting in a magnet, that can be magnetized best in the direction of the easy axis. ¹

In contrast to this, isotropic permanent magnets are produced without an applied external field. Thus they are cheaper and have no preferred direction, i.e., they can be magnetized in all directions alike (see Figure 1(a)). Since there exists no intrinsic anisotropy axis of the material, it is important to take the magnetization process into

¹Images taken from <http://www.simotecthailand.co.th/en/knowledge6.html>

account when simulating because it has a strong influence on the final remanent magnetization. The remanence is the magnetization that is left when the external field is turned off.

The simulations of permanent magnets require the nonlinear part of a hysteresis curve as input and therefore need to take the hysteretic material behavior into account. Isotropic and anisotropic magnets have different properties of hysteresis and this has to be considered in simulations.[3]

Since the magnetization process, that has to be considered when simulating isotropic magnets, is of vectorial nature, scalar models of hysteresis are insufficient.[4] Vector hysteresis models have to be considered instead. Although these vector hysteresis models are accurate for the simulation of isotropic magnets, they often involve large computational effort which reduced its application to medium scale problems.

Thus, a simpler model - the so-called freezing model was introduced to simulate isotropic magnets accurately.

The motivation of the freezing model is the following. The easy axes of the particles within an isotropic magnet are orientated randomly. Thus there is no homogeneous remanence magnetization within isotropic magnets since only the average magnetization is considered. Thus, magnetizing the isotropic magnet with inhomogeneous fields leads to inhomogeneous remanence states. For this reason simulations of isotropic magnets with homogeneous remanence magnetization lead to qualitatively wrong results compared to measurements of isotropic magnets.

Classical models that consider homogeneous remanence magnetization don't work in this case. The freezing model on the other hand considers inhomogeneous remanence magnetization.

It has been shown that after the magnetization process of isotropic magnets, the final remanence magnetization is not completely in z-direction but is slightly rotated. The freezing model considers this rotation of the magnetization vectors (see Figure 2).

The structure of this work is as follows.

First, in Chapter 1, the difference between soft and hard magnetic materials will be worked out and equations to model the different magnetic materials will be introduced. Additionally, different hysteresis models will be explained to give an insight to this topic. Then, the freezing condition will be introduced and it will be explained why it is needed for simulating isotropic magnets.

In the next chapter the freezing condition is compared to a simulation with an anisotropic material law and similarities as well as differences are pointed out.

After this, in Chapter 4, a computer experiment is performed to theoretically determine the freezing field H_{freeze} .

In the last part of this work, the simulations are compared to measurements that were done in a joint work with Infineon Austria and the Magnetfabrik Bonn.

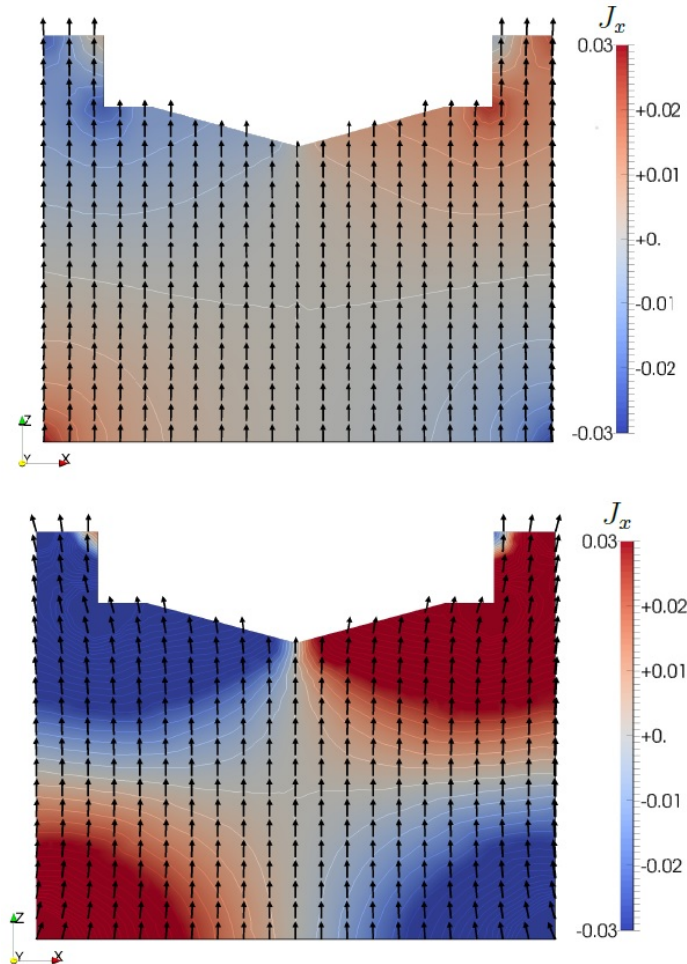


Figure 2: (Top) Simulation results using an anisotropic model. The resulting magnetic polarization shows weak flower state, but all magnetic moments are mostly aligned with the prescribed preferred direction. (Bottom) Simulation of isotropic magnet including the freezing condition and using a freezing field $\mu_0 H_{freeze} = 0.6\text{T}$. The applied field is gradually reduced from 4T to 0T until the final remanence state is reached. The final magnetic polarization shows the resulting flower state. ²

²Image taken from [2]

2 Modelling Magnetic Materials

Magnetic materials are metals with magnetic properties which are used for many applications like magnetic tapes, recording devices or generators. Thus, it's necessary to simulate the different types of magnetic materials correctly. The simulations are based on Maxwell's equations coupled with the constitutive relations. Since magnetic properties of different materials respond differently to a magnetic field, the material has to be simulated correctly in order to get an accurate simulation for the application. The two broad groups of magnetic materials are soft and hard magnetic materials. In this chapter an overview about these groups of magnets is given and equations to simulate them are presented. Furthermore the most common models of hysteresis are explained.

2.1 Hysteresis

One big difference between soft and hard magnetic materials is their hysteretic behavior. For this reason, hysteresis is shortly explained in this section.

Hysteresis is a property of ferromagnetic materials which describes the effect that the magnetization of a ferromagnetic material is not proportional to the applied external magnetic field but also depends on the prehistory of the material.[5] When an external field is applied to a magnet, the magnetization first increases proportional to the applied field until the magnetization reaches saturation. [6] If the external field is then decreased, the magnetization does not longer decrease proportional to the applied field. Indeed, if the applied field is turned off, there is some magnetization left, the so-called remanence magnetization. To get zero magnetization again, the external field must be applied in the opposite direction. The applied field at which the magnetization is zero again is called the coercivity field H_c .

Mathematically, hysteresis can be defined as by Bernotti and Mayergoz [7] using the language of control theory:

A transducer that is characterized by an input $x(t)$ and an output $y(t)$ is called hysteresis transducer if the input-output relationship is a multibranch non-linearity for which branch-to-branch transitions occur after an input extreme.[7]

Applying an alternating magnetic field to the material, the magnetization will trace out a loop. This nonlinear curve that plots the current magnetization as magnetization M against the external magnetic field H , is called a hysteresis curve (see Figure 3). From the hysteresis curve, the remanent magnetization \mathbf{M}_r , the coercivity field \mathbf{H}_c as well as the saturation magnetization \mathbf{H}_s can be seen.

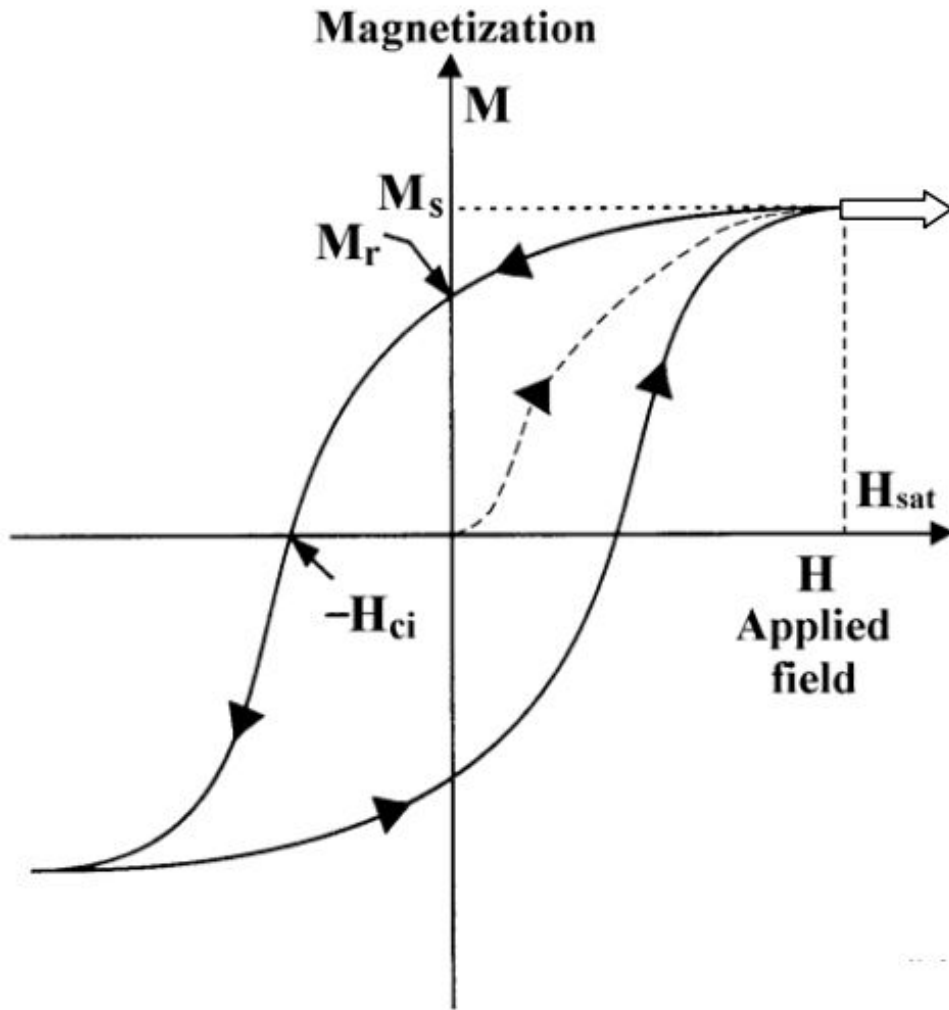


Figure 3: Hysteresis curve showing the magnetization M dependent on the applied field H . The magnetization is first driven to saturation. Then the applied field is decreased to zero, showing that there is remanent magnetization left when the field is turned off. Following this, the external field is applied in the opposite direction and driven to saturation again. At the coercivity field H_c the magnetization is zero. When applying an alternating magnetic field the magnetization of the material follows the nonlinear hysteresis curve. ³

From the hysteresis curve the "history" - dependence of the magnetization of ferromagnetic materials can be seen. If the magnetization is driven to saturation with the help of an applied field and the external field is then turned off, the magnet retains most of the magnetization and thus remembers the history in some way.

³Image taken from [8]

2.2 Soft Magnetic Materials

Soft magnetic materials are characterized by having a very low intrinsic coercivity H_{ci} , typically less than $100 \frac{\text{A}}{\text{m}}$. [9] They can be easily magnetized and demagnetized and do not have a high remanent magnetization. Thus, they are not used as permanent magnets but to enhance and channel the flux \mathbf{B} produced by an electric current. These transport applications require that the induced flux \mathbf{B} follows the primary field \mathbf{H} as closely as possible, i.e., a soft magnet should fulfill $\mathbf{B} = \mu\mathbf{H}$ and there should be no hysteresis (see Figure 4). Although a curve without any hysteresis does not exist, soft magnetic materials have a narrow hysteresis curve due to the low values of coercivity and remanence.

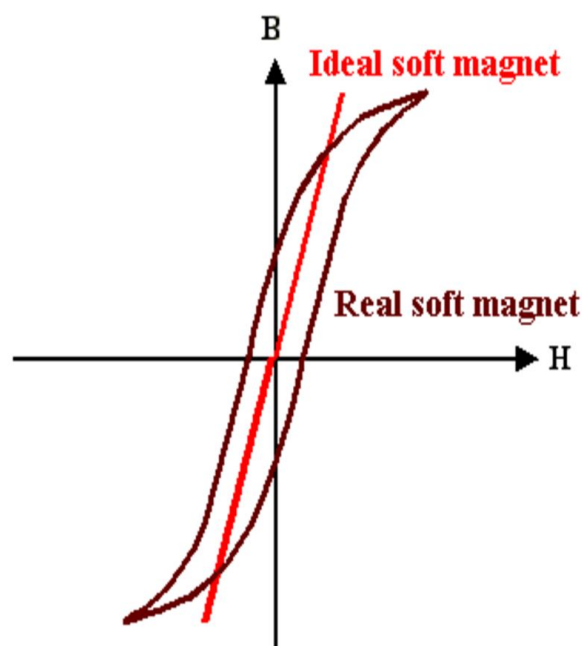


Figure 4: Hysteresis curve of soft magnets: The ideal soft magnet has no hysteresis, meaning that the hysteresis loop is just a linear line. In contrast to this a real soft magnet does have hysteresis and thus there is a hysteresis curve, although it is much slimmer than for hard magnetic materials. ⁴

The area of the hysteresis loop is proportional to the energy that is lost due to hysteresis. Different types of losses influence the energy loss of a magnet.

The hysteresis loss which is proportional to the area contained within the hysteresis loop can be reduced by choosing a material with lower intrinsic coercivity. Additionally to hysteresis losses the energy loss is affected by eddy current losses. Eddy currents are induced currents within the magnetic material.[6] These eddy currents lead to resistive

⁴Image taken from H. Föll: http://www.tf.uni-kiel.de/matwis/amat/elmat_en/kap_4/backbone/r4_3_6.html

losses. Eddy current losses can be reduced by choosing a material with low electrical conductivity. Lastly, there are anomalous losses which result from movements of domain walls within a material. To avoid these movements of domain walls, a material with homogeneous material can be chosen.

The types of applications for which soft magnets are used, require a high permeability μ . [9] Permeability describes the ability of the material to let magnetic fields pass through itself. Thus one of the most important parameters to characterize soft magnets is the relative permeability $\mu_r = \frac{B}{\mu_0 H}$.

As already mentioned, magnetic field formulation problems are described by Maxwell's equations, which can either be written in differential or in integral form. In the following, both types of equations are explained.

2.2.1 General Differential Formulation of Maxwell's Equations

Maxwell's equations are partial differential equations that are used to describe the fundamentals of electricity and magnetism.

The precise formulation of Maxwell's equations depends on the precise definition of the quantities involved. The equations consist of Gauss' law for electricity, Gauss' law of magnetism, Faraday's law of induction and Ampere's law . [11] The SI unit - formulations of Maxwell equations in free space are the following:

The Gauss' law for electricity

$$\nabla \cdot \mathbf{E} = \frac{\rho}{\epsilon_0} \quad (2.1)$$

describes how an electrical field behaves around electrical charges. Particularly, it states that the electrical field that leaves a volume is proportional to the charge inside.

$$\nabla \cdot \mathbf{B} = 0 \quad (2.2)$$

is the Gauss' law of magnetism and describes the non-existence of magnetic monopoles, since the total magnetic flux through a closed surface is zero (see Figure 5).

Faraday's law of induction describes that electric currents cause magnetic fields and vice versa magnetic field around a circuit give rise to electrical currents. It reads as

$$\nabla \times \mathbf{E} = -\frac{\partial \mathbf{B}}{\partial t} \quad (2.3)$$

Lastly, Ampere's law

$$\nabla \times \mathbf{B} = \mu_0 \left(\mathbf{J} + \epsilon_0 \frac{\partial \mathbf{E}}{\partial t} \right) \quad (2.4)$$

state that electric currents and changes in electric fields are proportional to the magnetic fields that circles around the current.

If Maxwell's equations are formulated in magnetic material, Gauss' law of electricity and Ampere's law have to be modified and constitutive equations have to be introduced.

In magnetic material, the formulation of Gauss' law of electricity becomes

$$\nabla \cdot \mathbf{D} = \rho \quad (2.5)$$

where \mathbf{D} in the general case fulfills

$$\mathbf{D} = \epsilon_0 \mathbf{E} + \mathbf{P} \quad (2.6)$$

In free space there holds $\mathbf{D} = \epsilon_0 \mathbf{E}$.

Ampere's law on the other hand reads as follows in magnetic material

$$\nabla \times \mathbf{H} = \mathbf{J} + \frac{\partial \mathbf{D}}{\partial t} \quad (2.7)$$

Here the constitutive equation in the general case is

$$\mathbf{B} = \mu_0 \mu_r (\mathbf{H} + \mathbf{M}) \quad (2.8)$$

In free space the constitutive equation simplifies to $\mathbf{B} = \mu_0 \mathbf{H}$

In the former equations the following notations are used

- \mathbf{E} ... electrical field, $[\frac{\text{V}}{\text{m}}]$
- \mathbf{B} ... magnetic field, $[\text{T}]$
- \mathbf{H} ... magnetic field strength, $[\frac{\text{A}}{\text{m}}]$
- \mathbf{D} ... electrical displacement, $[\frac{\text{C}}{\text{m}^2}]$

- \mathbf{M} ... magnetization, [$\frac{\text{A}}{\text{m}}$]
- \mathbf{P} ... polarization, [T]
- ϵ_0 ... permittivity of free space, [$\frac{\text{F}}{\text{m}}$]
- μ_0 ... permeability of free space, [$\frac{\text{H}}{\text{m}}$]
- μ_r ... relative permeability, dimensionless
- \mathbf{J} ... electric current density (current per unit area), [$\frac{\text{A}}{\text{m}^2}$]
- ρ ... electric charge density (charge per unit volume), [$\frac{\text{C}}{\text{m}^3}$]
- ∇ ... gradient
- $\nabla \cdot \dots$ divergence
- $\nabla \times \dots$ curl operator

The interface boundary conditions which can be derived from Maxwell's equations read as [12]

$$\mathbf{n} \times (\mathbf{H}^+ - \mathbf{H}^-) = 0 \quad (2.9)$$

$$\mathbf{n} \cdot (\mathbf{B}^+ - \mathbf{B}^-) = 0 \quad (2.10)$$

where the superscripts + and - are used for the physical quantities in the region of the ferromagnetic core V^+ and the region V^- external to V^+ . \mathbf{n} denotes the outer normal of the boundary on which the jump conditions are defined.

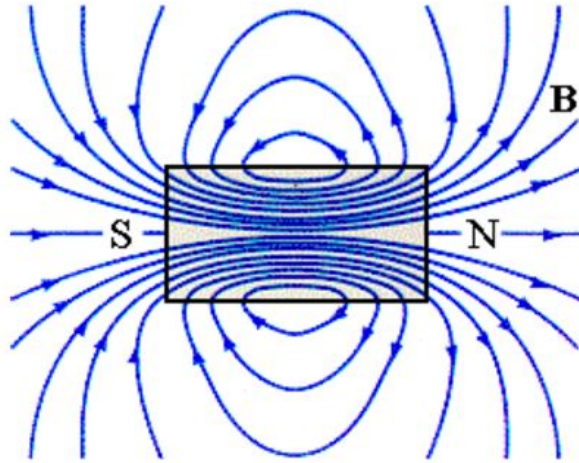


Figure 5: Depiction of Gauss' law of magnetism, showing the non-existence of magnetic monopoles and that magnetic field lines are closed loops. ⁵

2.2.2 Magnetostatic Maxwell Equations

The magnetostatic Maxwell equations with constitutive equations and the jump condition at the boundary are given by [1]

$$\text{rot } \mathbf{H} = \mathbf{j}, \quad \mathbf{B}^+ = \mu^+ \mathbf{H}^+ \quad (2.11)$$

$$\text{div } \mathbf{B} = \mathbf{0}, \quad \mathbf{B}^- = \mu^- \mathbf{H}^- \quad (2.12)$$

$$\mathbf{n} \times (\mathbf{H}^+ - \mathbf{H}^-) = \mathbf{0} \quad (2.13)$$

$$\mathbf{n} \cdot (\mathbf{B}^+ - \mathbf{B}^-) = 0 \quad (2.14)$$

where the current density \mathbf{j} is the source of the magnetic field strength \mathbf{H} which is related to the magnetic flux \mathbf{B} via the permeability μ .

2.2.3 Reduced Scalar Potential Formulation for Soft Magnets

Vector magnetic potentials are very useful for many applications. However, they are difficult to compute and for 3D magnetostatic Maxwell equations, it is useful to introduce a reduced scalar magnetic potential to simplify the computation. [12] The reduced scalar potential is a continuous and single-valued function in the whole space. It also helps to decrease the number of degrees of freedom in the computation.[1]

⁵Image taken from Dr. C. L. Davis: http://www.physics.louisville.edu/cldavis/phys299/notes/mag_monopoles.html

Introducing a reduced scalar potential u and writing

$$\mathbf{H} = \mathbf{H}_{\text{ext}} - \nabla u \quad (2.15)$$

the solution of Maxwell's equations can be reduced to the solution of scalar equations. No further assumptions are needed since the scalar potential is always well-defined. This equation naturally fulfills Faraday's law of induction.

Together with the constitutive equation $\mathbf{B} = \mu\mathbf{H}$ which describes the relationship between the magnetic field intensity and the flux density \mathbf{B} the equations are

$$\nabla \cdot (\mu^+ \nabla u^+) = \nabla \cdot (\mu^+ \mathbf{H}_{\text{ext}}) \quad (2.16)$$

$$\nabla^2 u^- = 0 \quad (2.17)$$

$$u^+ - u^- = 0 \quad (2.18)$$

$$\mu^+ u^+ - \mu^- u^- = (\mu^+ - \mu^-) \mathbf{n} \cdot \mathbf{H}_{\text{ext}} \quad (2.19)$$

This formulation has no restriction on geometry but there is one big drawback, namely that cancellation errors can occur. [13] These errors happen when $\mathbf{H} = \mathbf{H}_{\text{ext}} - \nabla u$ is used to calculate the magnetic field \mathbf{H}^+ within the ferromagnetic core. Due to the iron within the ferromagnetic core the magnitude of \mathbf{H}_{ext} and $-\nabla u$ are almost equal but the directions are opposite and the two contributions nearly cancel out, which may lead to large numerical errors.

A way to get around this problem is to use a total scalar potential field.

2.2.4 Total Scalar Potential Formulation for Soft Magnets

In this formulation the condition

$$\mathbf{H}^- = \mathbf{H}_{\text{ext}} - \nabla u^- \quad (2.20)$$

is only used to compute the magnetic field in the region V^- whereas in the ferromagnetic core the field is described by the equation [12]

$$\mathbf{H}^+ = -\nabla \tilde{u}^+ \quad (2.21)$$

The equations and boundary conditions for $\mathbf{B} = \mu\mathbf{H}$ under the assumption that there are no currents within the magnetic region then read as

$$\nabla \cdot (\mu^+ \nabla \tilde{u}^+) = 0 \quad (2.22)$$

$$\nabla^2 u^- = 0 \quad (2.23)$$

$$\tilde{u}^+ - u^- = u_{ext} \quad (2.24)$$

$$\mu^+ \frac{\partial \tilde{u}^+}{\partial n} - \mu^- \frac{\partial u^-}{\partial n} = -\mu^- \mathbf{n} \cdot \mathbf{H}_{ext} \quad (2.25)$$

where u_{ext} is a scalar magnetic potential of the external field \mathbf{H}_{ext} . The total potential formulation is only possible in regions without currents since the total field cannot always be written as $\mathbf{H}_{tot} = \nabla u$ because of $\text{rot}(\mathbf{H}_{tot}) = j$.

With the total scalar potential formulation, the problem of cancellation errors can be avoided. However, the potential is a discontinuous potential across the iron-air interface and the formulation only holds for simply connected geometries.

2.2.5 Solving Maxwell's Equations

The reduced scalar potential formulation of Maxwell's equations can numerically be solved by using the direct Johnson-Nédélec FEM-BEM coupling method as pointed out by Bruckner et al.[1]. This method uses Finite Element Method (FEM) to treat the magnetostatic problem within the magnetic material. In contrast to this, Boundary Element Method (BEM) is used for the region outside of the magnetic material. With BEM, volume integrals, that come from the open boundary problem, can be transformed to corresponding surface integrals due to the missing magnetic sources in the outer region.

Combining these two methods gives the advantages of both methods. The non-linearity of the problem can efficiently be treated with FEM. BEM transforms the boundary condition from infinity to the surface of the magnet and therefore no finite elements are required outside of the magnets to solve the system correctly.

The discretization yields the following system of equations [2]

$$\begin{pmatrix} M_{ij}^{11} & M_{in}^{12} \\ M_{mj}^{21} & M_{mn}^{22} \end{pmatrix} \begin{pmatrix} u_j \\ \phi_n \end{pmatrix} = \begin{pmatrix} RHS_i^1 \\ 0 \end{pmatrix} \quad (2.26)$$

$$M_{ij}^{11} = \int_{\Omega} \nabla \Lambda_i \cdot \mu \cdot \Lambda_j d\Omega \quad (2.27)$$

$$M_{in}^{12} = - \int_{\Gamma} \Lambda_i \mathbb{1}_n d\Gamma \quad (2.28)$$

$$M_{mj}^{21} = \frac{1}{2} \Lambda_j(x_m) - \frac{1}{4\pi} \int_{\Gamma} \Lambda_j(y) \frac{x_m - y}{|x_m - y|^3} \mathbf{n} d\Gamma_y \quad (2.29)$$

$$M_{mn}^{22} = \frac{1}{4\pi} \int_{\Gamma} \frac{\mathbb{1}_n(y)}{|x_m - y|} d\Gamma_y \quad (2.30)$$

$$RHS_i^1 = \int_{\Omega} (\mathbf{H}_{ext} \cdot \mu + \mathbf{B}_r) \cdot \nabla \Lambda_i d\Omega - \int_{\Gamma} \mathbf{H}_{ext} \cdot \mathbf{n} \Lambda_i d\Gamma \quad (2.31)$$

These equations can be solved with a Newton-Krylov solver. Newton-Krylov solvers are used to numerically solve non-linear PDEs. These solvers use Newton's method as a basic solver and then a Krylov-subspace method to solve the system of linear equations. One method of the class of Newton-Krylov methods are GMRES methods. GMRES method is an iterative numerical method to solve large sparse systems of linear equations. One special solver that uses Newton-Krylov method is the KINSOL solver.[14]

2.2.6 Integral Formulation of Maxwell's Equations

Since the differential Maxwell's equations hold for every point $x \in \Omega$ the equations can be intergrated over any volume V or through any surface and still remain true. Here Ω is the region where the problem is defined. By using the divergence theorem and the Stokes' theorem, the integral formulations of Maxwell's equations in free space are [6]

Gauss' law of electricity

$$\oiint_S \mathbf{E} \cdot d\mathbf{S} = \frac{1}{\epsilon_0} \iiint_V \rho dV = q \quad (2.32)$$

Gauss' law of magnetism

$$\oiint_S \mathbf{B} \cdot d\mathbf{S} = 0 \quad (2.33)$$

Faraday's law of induction

$$\oint_L \mathbf{E} \cdot dL = - \iint_S \frac{\partial \mathbf{B}}{\partial t} \cdot dS \quad (2.34)$$

Ampère's circuital law

$$\oint_L \mathbf{B} \cdot dL = \iint_S \mu_0 \mathbf{J} \cdot dS + \iint_S \mu_0 \epsilon_0 \frac{\partial \mathbf{E}}{\partial t} \cdot dS \quad (2.35)$$

As before, the Gauss' law of electricity and the Ampère's circuital law need to be modified in order to define them for magnetic material.

Gauss' law of electricity in magnetic material reads then as

$$\oiint \mathbf{D} \cdot dS = \iiint \rho \, dV \quad (2.36)$$

where \mathbf{D} is given again by

$$\mathbf{D} = \epsilon_0 \mathbf{E} + \mathbf{P} \quad (2.37)$$

Ampère's circuital law in magnetic material is given by

$$\oint_L \mathbf{H} \cdot dL = \iint_S \mathbf{J} \cdot dS + \iint_S \frac{\partial \mathbf{D}}{\partial t} \cdot dS \quad (2.38)$$

with the constitutive equation

$$\mathbf{B} = \mu_0 \mu_r (\mathbf{H} + \mathbf{M}) \quad (2.39)$$

In Gauss' law of electricity and Gauss' law of magnetism, S is a closed surface that encloses a 3D volume.

In Faraday's and Ampere's law, S denotes an open surface that has a boundary line L . The notation is the same as in Section 2.2.1.

2.2.7 Method of Moments

An alternative approach to solve magnetic field formulation problems and model electrotechnical devices is the so-called Method of Moments (MoM). [15] This method was developed more than 30 years ago by R.F. Harrington and appears as an alternative to classical FEM in some cases.

The main idea of this method is that, in contrast to classical FEM, no mesh is needed in free space. Only the material parts that are ferromagnetic are divided into elementary parts. These elements are called moments and with each of them, a uniform magnetization is associated.

In MoM it is assumed that the magnetic field is created by the inductor source and all the moments defined in the problems.

It can be seen in the paper of Chadebec, Coulomb and Janet [15] that a magnetostatic problem composed of some ferromagnetic regions and coils in which currents flow is considered. The equations describing the problems are

$$\operatorname{div} \mathbf{B} = 0 \quad (2.40)$$

$$\operatorname{curl} \mathbf{H} = \mathbf{J} \quad (2.41)$$

and the classical material law

$$\mathbf{M}_{\text{ind}} - \mathbf{M}_{\text{rem}} = f(\mathbf{H})\mathbf{H} \quad (2.42)$$

In these equations \mathbf{M}_{ind} is the induced magnetization of the material, whereas \mathbf{M}_{rem} is the permanent magnetization. \mathbf{J} denotes the electric current density.

As before, a reduced scalar potential can be used to write

$$\mathbf{H} = \mathbf{H}_{\text{ext}} - \nabla u \quad (2.43)$$

where \mathbf{H}_{ext} fulfills $\operatorname{curl} \mathbf{H}_{\text{ext}} = \mathbf{J}$.

The reduced scalar potential is equal to

$$u = \frac{1}{4\pi} \iiint_V \frac{(\mathbf{M}_{\text{ind}} + \mathbf{M}_{\text{rem}}) \cdot \mathbf{r}}{r^3} dV \quad (2.44)$$

where V is the volume of ferromagnetic material and \mathbf{r} is the vector between the

integration point and the point P where the field is expressed.

Calculating the gradient and plugging in the term in the reduced scalar potential formulation yields for the magnetic field \mathbf{H}

$$\begin{aligned} \mathbf{H} = & \mathbf{H}_{\text{ext}} + \frac{1}{4\pi} \iiint_V \left(\frac{3(\mathbf{M}_{\text{ind}} \cdot \mathbf{r})}{r^5} \mathbf{r} - \frac{1}{r^3} \mathbf{M}_{\text{ind}} \right) dV \\ & + \frac{1}{4\pi} \iiint_{V_{\text{magnet}}} \left(\frac{3(\mathbf{M}_{\text{rem}} \cdot \mathbf{r})}{r^5} \mathbf{r} - \frac{1}{r^3} \mathbf{M}_{\text{rem}} \right) dV \end{aligned} \quad (2.45)$$

To find a good discretization of the problem, it is assumed that the modeled device is composed of several magnets (V_{magnet}) with a known magnetization \mathbf{M}_{rem} , inductors in which static currents \mathbf{I} flow and ferromagnetic parts (V) with unknown magnetization \mathbf{M}_{ind} .

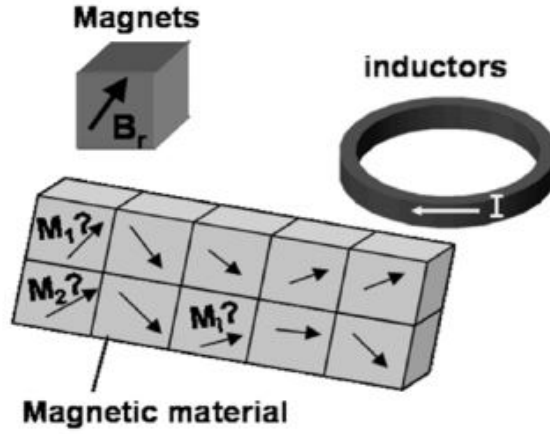


Figure 6: Device that is studied including magnets, inductors and ferromagnetic parts which are meshed into volume elements. ⁶

Dividing the ferromagnetic material into N volume elements and the magnets into K volume elements and assuming that the magnetizations are uniform in each element of the ferromagnetic materials and in the magnet, results in the equation

$$\begin{aligned} \mathbf{H} = & \mathbf{H}_{\text{ext}} + \frac{1}{4\pi} \sum_{n=1}^N \iiint_{V_n} \left(\frac{3(\mathbf{M}_{\text{ind}_n} \cdot \mathbf{r})}{r^5} \mathbf{r} - \frac{1}{r^3} \mathbf{M}_{\text{ind}_n} \right) dV_n \\ & + \frac{1}{4\pi} \sum_{k=1}^K \iiint_{V_{\text{magnet}_k}} \left(\frac{3(\mathbf{M}_{\text{rem}_k} \cdot \mathbf{r})}{r^5} \mathbf{r} - \frac{1}{r^3} \mathbf{M}_{\text{rem}_k} \right) dV_k \end{aligned} \quad (2.46)$$

⁶Image taken from [15]

Since the discrete equation (2.39) is linear, it can be rewritten with the help of the definition of an orthogonal basis in each volume element as follows

$$\mathbf{H} = \mathbf{H}_{\text{ext}} + \mathbf{G}[\mathbf{m}_{\text{rem}}] + \mathbf{F}[\mathbf{m}_{\text{ind}}] \quad (2.47)$$

where \mathbf{G} is a $(3 \times 3K)$ matrix and \mathbf{F} is a $(3 \times 3J)$ matrix. $[\mathbf{m}_{\text{rem}}]$ is a $(3K \times 1)$ vector whereas $[\mathbf{m}_{\text{ind}}]$ is a $(3J \times 1)$ vector and these coefficients define the magnetizations in each local basis.

In MoM the discrete points that are chosen are the barycenters of each element.

An approximate solution of (2.38) can then be obtained by the Point-Matching Method. The idea of this method is that the approximate solution should fulfill the equation (2.40) at discrete points in the region of interest and is then projected in its local basis.

In the matter of a linear ferromagnetic material law, the relation between the magnetization and the field is

$$\mathbf{M}_{\text{ind}} = (\mu_r - 1) \mathbf{H} \quad (2.48)$$

Combining equation (2.41) with the discrete equation (2.40) in an orthogonal basis, leads to the linear system

$$(\mathbf{Id} - \mathbf{F})[\mathbf{m}_{\text{ind}}] = [\mathbf{h}_0] + \mathbf{G}[\mathbf{m}_{\text{rem}}] \quad (2.49)$$

Here \mathbf{G} and \mathbf{F} are global square matrices and not local ones as before. This system has $3 \times J$ unknown. Here, \mathbf{Id} denotes the identity matrix and $[\mathbf{h}_0]$ is the source field at each barycenter projected in the local basis.

The main advantages of the moment method is that it does not require any mesh outside the ferromagnetic material just like FEM-BEM coupling. This leads to high-speed resolutions and to high accuracies for stray field computations. Additionally, nonlinear material law can be treated easily.[1] However, the main difficulty of MoM is the computation of the matrix coefficients of \mathbf{F} and \mathbf{G} . The moment method leads to square and dense systems which consume a lot of memory and often need too much time to be solved. Using FEM-BEM coupling leads to sparse matrices for the area where FEM is used. BEM also leads to dense systems, but only on the boundary and thus the matrices are smaller than for the moment method since only surface matrices are considered.

2.3 Hard Magnetic Materials

Hard magnetic materials have high values of intrinsic coercivity H_{ci} , often about $200 - 2000 \frac{\text{kA}}{\text{m}}$ and hence retain their magnetism even if the applied field is turned off.[9] Since it is difficult to demagnetize hard magnets after they have been magnetized once, they are widely used as permanent magnets.[10] Examples are magnetic separators, motors, loudspeakers or holding devices. The most common hard magnetic materials are aluminum-nickel-cobalt alloys, cobalt-samarium alloys, iron-chromium-cobalt alloys and neodymium-iron-boron alloys.

The high values of H_{ci} and the remanent magnetization B_r lead to a large hysteresis loop area (see Figure 7).

Hard magnetic materials are characterized by the so-called maximum energy product $(BH_{ci})_{max}$ which is proportional to the hysteresis loop area. The maximum energy product $(BH_{ci})_{max}$ is a measure for the maximal amount of energy that can be stored in a magnet. Magnets with higher maximum energy product $(BH_{ci})_{max}$ are stronger than magnets with lower $(BH_{ci})_{max}$. Thus, to get a good permanent magnet, a material with high maximum energy product should be chosen.

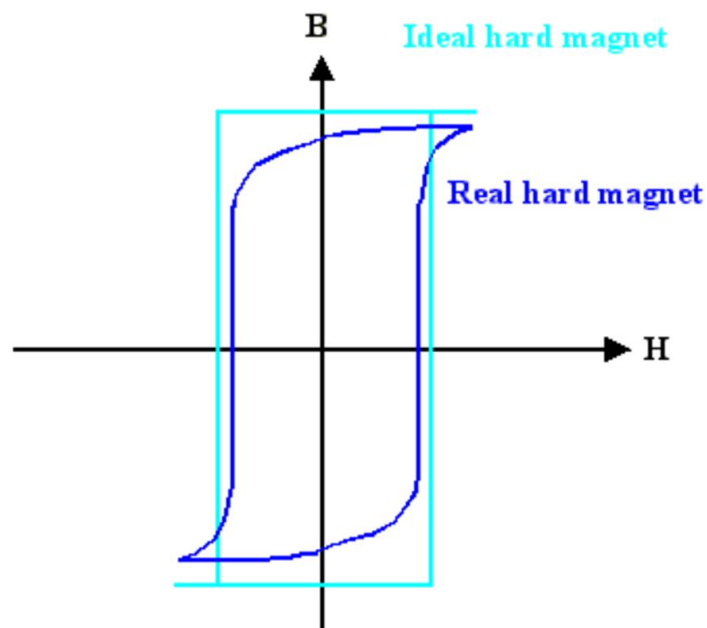


Figure 7: Hysteresis curve of ideal hard magnets in comparison to hysteresis curve of real hard magnet. ⁷

⁷Image taken from H. Föll: http://www.tf.uni-kiel.de/matwis/amat/elmat_en/kap_4/backbone/r4_3_6.html

For this reason, modeling of hard magnetic materials also requires the modeling of hysteresis. In the past, many models to describe magnetic hysteresis have been introduced. The most common models are presented after Maxwell's equations are modified for hard magnetic material.

2.3.1 Maxwell's Equations for Hard Magnets

In contrast to soft magnetic materials, the simulation of hard magnets require to take the remanence into account, leading to a different formulation of Maxwell's equations. The constitutive equation for hard magnetic materials is [13]

$$\mathbf{B} = \mu\mathbf{H} + \mathbf{B}_r \quad (2.50)$$

where \mathbf{B}_r is the remanent flux density and μ is the permeability.

For the magnetization \mathbf{M} there holds a modified material law

$$\mathbf{M} = \chi\mathbf{H} + \mathbf{M}_r \quad (2.51)$$

where χ is the susceptibility.

The equations for hard magnetic material with a reduced scalar potential u are then [2]

$$\mathbf{H} = \mathbf{H}_{\text{ext}} - \nabla u \quad (2.52)$$

$$\nabla \cdot (\mu^+ \nabla u^+) = \nabla \cdot (\mu^+ \mathbf{H}_{\text{ext}} + \mathbf{B}_r) \quad (2.53)$$

$$\nabla^2 u^- = 0 \quad (2.54)$$

$$u^+ - u^- = 0 \quad (2.55)$$

$$\mu^+ u^+ - \mu^- u^- = (\mu^+ - \mu^-) \mathbf{n} \cdot \mathbf{H}_{\text{ext}} + \mathbf{n} \cdot \mathbf{B}_r \quad (2.56)$$

As already presented before these equations can be numerically solved by the Newton - Krylow method. To handle the open-boundary problem correctly, Johnson - Nédélec FEM-BEM coupling is used.

2.3.2 Scalar Preisach Models

As mentioned before, simulations of hard magnets require modeling of hysteresis. One way of describing hysteresis are (scalar) Preisach models, which were first introduced by Ferenc Preisach in 1935. Preisach models describe a hysteresis loop as a connection of single units, the so-called hysterons. [16] These hysterons have a certain switching characteristic. The simplest hysteretic transducers are nonideal relays. These

fundamental building blocks are two-valued operators $R_{\alpha,\beta}$ with threshold value $\alpha < \beta$. [17] α hereby denotes a down-switching field and β an up-switching field. The output $y(t)$ of the transducer $R_{\alpha,\beta}$ can take the values 0 and 1, meaning that the relay is either switched off or switched on. The output $y(t)$ of $R_{\alpha,\beta}$ can be expressed as

$$R_{\alpha,\beta} = \begin{cases} 1 & x \geq \beta \\ 0 & x \leq \alpha \\ k & \alpha < x < \beta \end{cases} \quad (2.57)$$

where $k = 0$ if $x \leq \alpha$ the last time x was outside boundaries $\alpha < x < \beta$ and $k = 1$ if $x \geq \beta$ the last time x was outside boundaries $\alpha < x < \beta$.

The two magnetic states are stable as long as the applied field lies between α and β .

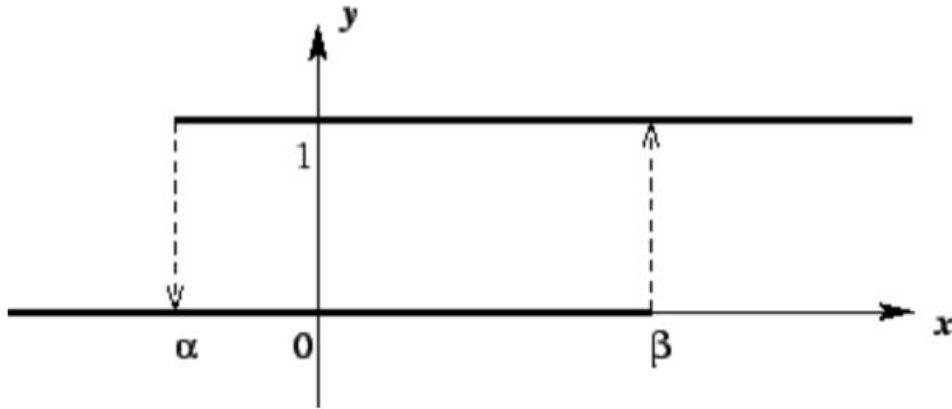


Figure 8: Nonideal relay with up down-switching field α and up-switching field β , and $\alpha < \beta$. ⁸

The hysteresis loop is then characterized as a parallel connection of these relay hysterons which are weighted and summed. It can be visualized in the following way. [18]

⁸Image taken from Alexei Pokrovskii: <http://euclid.ucc.ie/hysteresis/node9.htm>

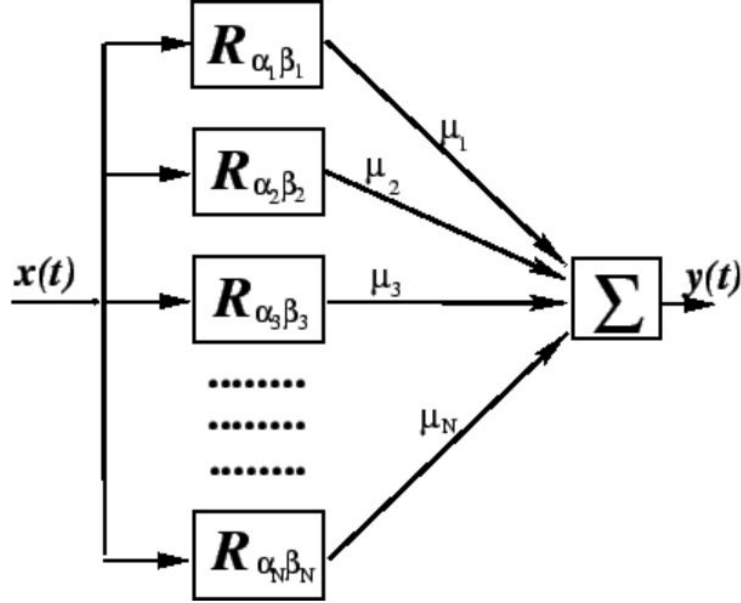


Figure 9: Weighted parallel connection of a finite number of nonideal relays. ⁹

Different relays have different threshold values α_i and β_i and are weighted by various μ_i , $i = 1, \dots, N$.

2.3.3 Vector Preisach Models

Although scalar Preisach models are progressively accurate and they describe scalar hysteresis very efficiently, they are limited by the congruency and the deletion property.[16] The congruency property states that in a classical Preisach model all minor loops between a pair of applied fields are congruent. Furthermore, the deletion property states that the effect of a minimum/maximum is deleted if it is followed by another minimum/maximum. [19]

Another drawback of scalar Preisach models is that they consider the magnetization only in the direction of the easy axis, i.e., only changes in the magnitude of the magnetization are considered. Since the magnetization process is of vectorial nature, the spatial change of the magnetization direction has to be taken into account. [2] Thus, vectorial hysteresis models have been developed to describe the magnetization process accurately.

These vector hysteresis models need to fulfill two additional properties, namely the saturation property and the loss property. The saturation property requires that if the applied field is large enough the magnetization can achieve saturation and that it cannot exceed saturation. The loss property on the other hand demands from the

⁹Image taken from Alexei Pokrovskii: <http://euclid.ucc.ie/hysteresis/node12.htm>

models to consider the fact that increasing the size of a rotating field first leads to an increase and then a decrease of losses.

The idea of a vector Preisach model which was introduced by Mayergoyz [18] is a model which consists of a continuum of scalar Preisach transducers, each incrementally rotated from its neighbor. The component of the applied field in the transducer's direction is the input to each transducer whereas the output of each transducer is the magnetization in this direction. The vector sum of the output of all transducers is then the complete model's output.

This vector Preisach model reduces to a scalar Preisach model when the change of magnetization is only one-dimensional, i.e., only the magnitude of the magnetization changes.

2.3.4 Stoner - Wohlfarth model

The Stoner - Wohlfarth (SW) model is a mathematical model describing hysteresis effects of ferromagnetic materials. It was postulated by Edmund C. Stoner and Erich P. Wohlfarth in 1948.[20] The Stoner - Wohlfarth model describes the vectorial behavior of one single-domain particle and is based on the idea that the magnetic momentum of single-domain particles rotates with respect to their easy axis.[21]

Each of these SW particles can be seen as an elementary vectorial hysteron and combining these hysterons like in a Vector - Preisach model gives a vectorial hysteresis model.

A Stoner - Wohlfarth particle (see Figure 10(a)) is a single-domain, uniaxial magnetic particle with a magnetic momentum \mathbf{m} . The anisotropy of each particle results from crystal structure, the particle shape or stress. The easy axis of one single-domain particle points in a prescribed direction.

The orientation angle ϕ of \mathbf{m} , which indicated the rotation of the resulting magnetization \mathbf{m} from the easy axis, can change under the influence of an applied field H_{ext} but the magnitude stays the same. By symmetry considerations, it is clear that the vector \mathbf{m} of the particle lies in the plain formed by the easy axis x and the applied magnetic field H_{ext} . [7] The orientation of the magnetic momentum of each particle naturally rotates to a state where minimal energy is needed.

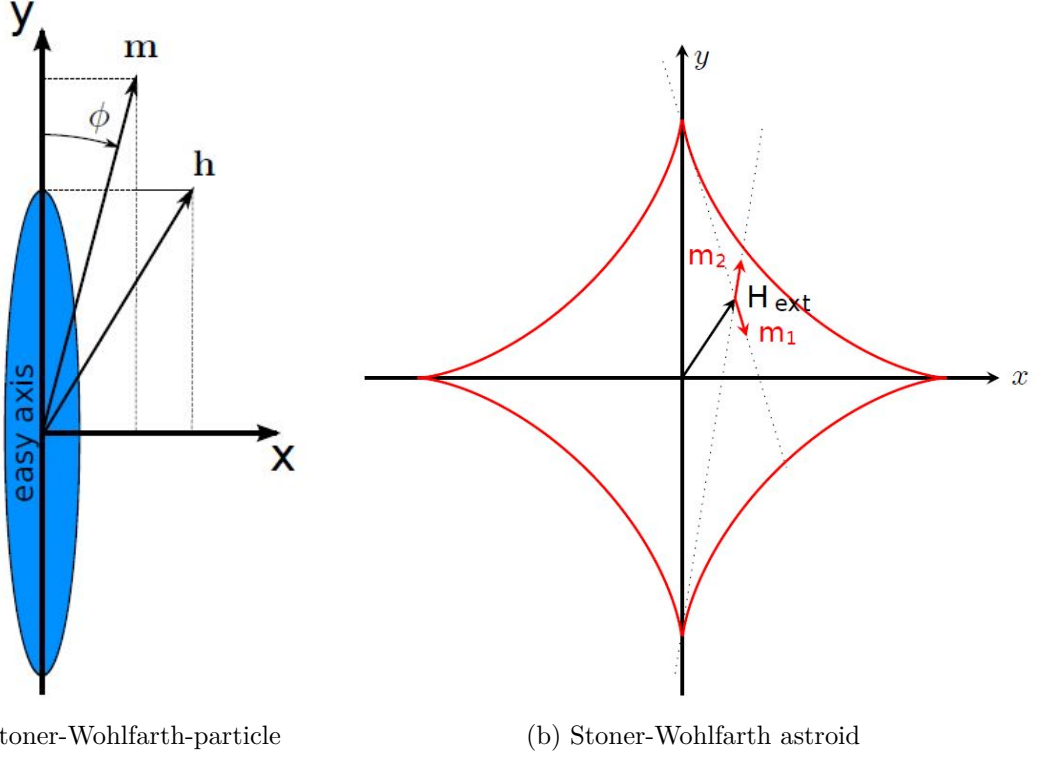


Figure 10: (Left) Stoner-Wohlfarth particle with uniaxial anisotropy with easy axis along the y -axis. The angles of the applied external field \mathbf{h} and the resulting magnetization \mathbf{m} are related to the easy axis. (Right) Stoner-Wohlfarth astroid for uniaxial anisotropy along y -axis. Outside of the astroid there is only one stable solution. Two stable solutions exist inside the astroid. These solutions can be constructed by tangents on the astroid passing through the tip of the applied field vector \mathbf{H}_{ext} . [24]¹⁰

The normalized total energy density of a Stoner - Wohlfarth particle consists of the anisotropy energy and the Zeeman energy and reads as given by Bertotti [22]

$$\eta = \frac{E}{2KV} = \frac{1}{2} \sin^2(\phi) - h_x \sin(\phi) - h_y \cos(\phi) \quad (2.58)$$

where E is the energy, $\mathbf{h} = \frac{\mathbf{H}}{H_k}$ is the normalized field and $H_k = \frac{2K}{\mu_0 M_s}$ is the anisotropy field.

Stable magnetization states can be calculated by minimizing the particle energy, i.e.,

$$\frac{\partial \eta}{\partial \phi} = \sin(\phi) \cos(\phi) - h_x \cos(\phi) + h_y \sin(\phi) = 0 \quad (2.59)$$

¹⁰Images taken from [24]

By transforming the equation to cartesian coordinates as pointed out by Wood [23] the condition reads

$$\frac{h_x}{m_x} - \frac{h_y}{m_y} = 1 \quad (2.60)$$

Since η is the normalized energy density, the normalized magnetization m has magnitude 1 and thus the condition

$$m_x^2 + m_y^2 = 1 \quad (2.61)$$

allows to eliminate either m_x or m_y , resulting in the following fourth order equation [24]

$$m_x^4 - 2H_x m_x^3 + (h^2 - 1)m_x^2 + 2h_x m_x - h_x^2 = 0 \quad (2.62)$$

or alternatively

$$m_y^4 + 2H_y m_y^3 + (h^2 - 1)m_y^2 - 2h_y m_y - h_y^2 = 0 \quad (2.63)$$

A quartic equation always has four solutions in the complex plane but not all of them have to be real.

The region where all four solutions are real can be separated from the region with only two real solutions by the critical curve given by

$$\frac{\partial^2 \eta}{\partial \phi^2} = 0 \quad (2.64)$$

This critical curve is called Stoner - Wohlfarth astroid (see Figure 10(b)). In other words, the Stoner - Wohlfarth astroid separates the region with two energy minima from this with only one minimum. Thus, with the Stoner - Wohlfarth astroid it is possible to explain both reversible and irreversible changes in magnetization.

For small fields the particle magnetization only has a small deviation from the easy axis and there are two energy minima m_1 and m_2 . When the magnetic field increases, the positions of the energy minima change.

In the beginning, these position changes are fully reversible. Nevertheless, once a certain critical field H_c is exceeded, the behavior of the minima changes.

One of the minima suddenly becomes unstable and the magnetization of the domain jumps to the other global minimum. This discontinuous change of magnetization occurs when the critical curve of the Stoner - Wohlfarth astroid is crossed and explains the irreversible magnetization change.

If the critical field is measured along different directions, it shows that the critical field differs along the hard- and the easy axis. This effect is not as expected by a simple SW-model, but can easily be integrated into the standard SW model by using a scaled field \mathbf{h}^* to a standard SW model, where only the y component is reduced (see Figure 11).

$$h_x^* = h_x \quad h_y^* = C h_y \quad (2.65)$$

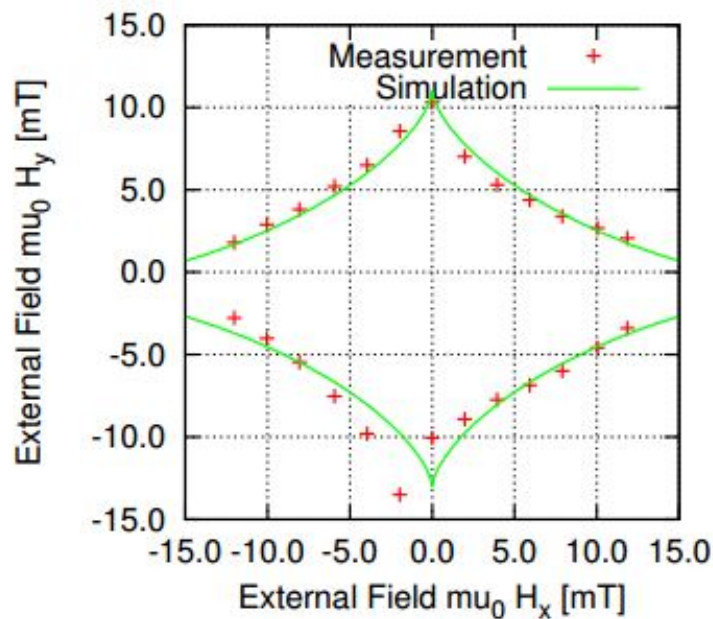


Figure 11: Measurement of the critical field of a GMR sensor for different field directions. The size of the particle is small enough to describe it via a Stoner-Wohlfarth model. The measurement shows that the saturation field along the hard-axis (24mT) is almost twice as high as the switching field along the easy axis (12mT). A scaled SW model, where only the y -component of the applied field is scaled, is used to fit the scales measurement data. [24] ¹¹

¹¹Image taken from [24]

The attractiveness of the Stoner - Wohlfarth model comes from its strong appeal to physical intuition and the fact that both the reversible and the irreversible magnetization changes can be explained by a single mechanism. The Stoner - Wohlfarth model is also naturally three dimensional and easily accounts for anisotropy.

However, there are also some simplifications of the Stoner - Wohlfarth model that may not be met in real life, for example no interactions between particles are assumed, pinning effects are not considered and each particle must consist of a single, uniformly magnetized domain. Additionally, the SW model does not describe non-symmetrical loops since it is constructed as a superposition of particles with symmetrical loops.[17]

2.3.5 Freezing Model

Vector hysteresis models, as the previously explained Vector-Preisach model or Jiles-Atherton models [25] are useful for the simulation of dynamic hysteresis effect, they often involve a large computational effort which is often not needed. For the simulation of permanent magnetic materials, the correct description of the hysteretic behavior near the saturation configuration is often sufficient. [2]

For the simulation of isotropic permanent magnets a new method for the description of hysteretic behaviour near the saturation state was introduced by Bruckner et al.[2] This method only uses a single parameter, the freezing field H_{freeze} , to calculate the remanence magnetization of isotropic magnets in a phenomenological way.

During the magnetization process the magnitude and the direction of the total magnetic field play an important role for the final remanent magnetization. If the applied field is large enough, the average magnetic moment within the magnet points in the direction of the total field. This total field is spatially varying and the \mathbf{B}_r -vector gets more and more inhomogeneous when the applied field is reduced. The variation of the \mathbf{B}_r -vector finally freezes if the magnitude of the total field is below a certain threshold.

This shape dependence of the \mathbf{B}_r indicates that the magnetization process needs to be considered in the simulation.

For this reason, the so called freezing condition $|\mathbf{H}| > H_{freeze}$ for a critical freezing field H_{freeze} is introduced and checked in each timestep. After each check the \mathbf{B}_r -vector is updated by the condition

$$\mathbf{B}_r = \begin{cases} |\mathbf{B}_r| \frac{\mathbf{H}}{|\mathbf{H}|} & \text{if } |\mathbf{H}| > H_{freeze} \\ \mathbf{B}_r & \text{otherwise} \end{cases} \quad (2.66)$$

The \mathbf{B}_r -vector is perfectly aligned with a prescribed direction in the beginning.

The applied field is decreased step by step and the total field is calculated by

$$\mathbf{H} = \mathbf{H}_{\text{ext}} - \nabla u \quad \text{in } \Omega \quad (2.67)$$

$$\nabla \cdot (\mu \nabla u) = \nabla \cdot (\mu \mathbf{H}_{\text{ext}} + \mathbf{B}_r) \quad \text{in } \Omega \quad (2.68)$$

$$\Delta u = 0 \quad \text{in } \mathbb{R}^3 \setminus \Omega \quad (2.69)$$

$$[[u]] = 0 \quad \text{on } \partial\Omega \quad (2.70)$$

$$[[\nabla u \cdot \mu \cdot \mathbf{n}]] = (\mathbf{H}_{\text{ext}} \cdot [[u]] + \mathbf{B}_r) \cdot \mathbf{n} \quad \text{on } \partial\Omega \quad (2.71)$$

where u is a reduced scalar potential, $[[\cdot]]$ denotes the jump of a quantity over the boundary $\partial\Omega$ of the magnetic domain and \mathbf{n} is the outward pointing surface unit normal.

The aim is now to detect H_{freeze} . Taking into account that the magnetic grains can be simulated by a Stoner-Wohlfarth model, it is expected that H_{freeze} fulfills the condition [2]

$$\frac{H_k}{2} < H_{\text{freeze}} < H_k \quad (2.72)$$

Here, H_k is the anisotropy field of the individual particle.

This is because a field larger than the anisotropy field is strong enough to align all magnetization vectors into the correct half-sphere, i.e., in the half-sphere in which the applied field is pointing. The second inequality results from the fact that $\frac{H_k}{2}$ is the minimal switching field. That means that for $H < \frac{H_k}{2}$ there are no irreversible processes, implying that M_r is frozen in any case.

A motivation of the freezing model is the problem that ANSYS simulations performed at Infineon¹² sensors including isotropic permanent magnets showed qualitatively different behavior than the measurement data of these magnets. This can be seen in Figure 12. The freezing condition was then included in the simulations and with a freezing field of $\mu_0 H_{\text{freeze}} = 0.6\text{T}$ the simulations match with the measurement data.

¹²Infineon Austria

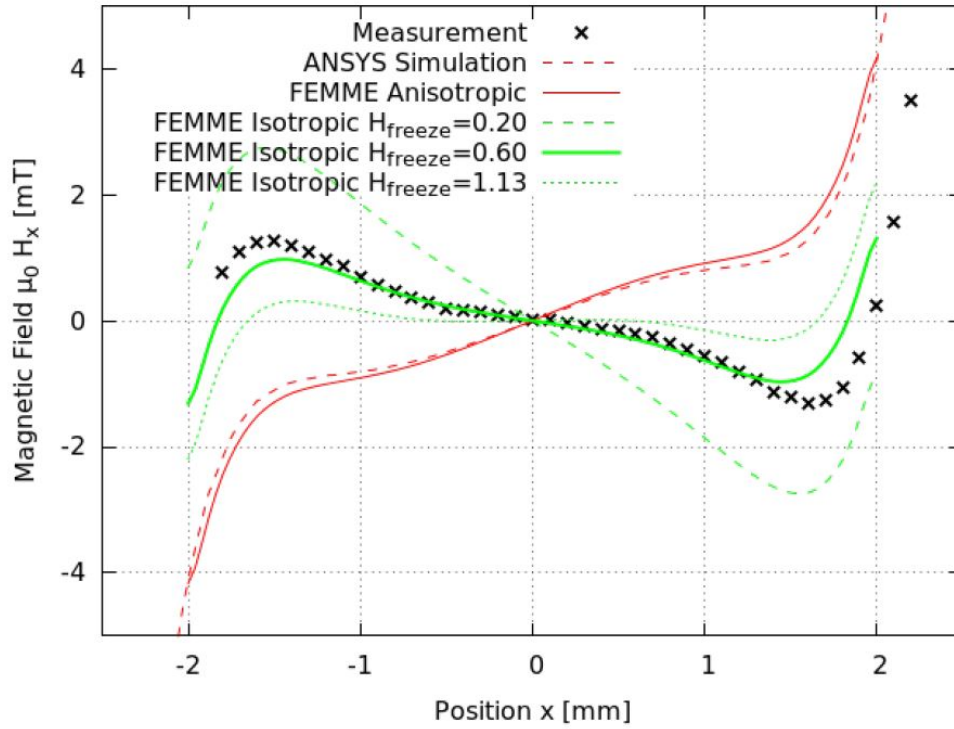


Figure 12: Comparison of strayfield measurement with different simulations of isotropic magnets: (a) ANSYS simulation as well as (b) FEMME assuming an anisotropic material law. (c) FEMME simulation including the freezing condition with different freezign fields $\mu_0 H_{freeze} = 0.2/0.6/1.13\text{T}$.¹³

¹³Image taken from [2]

3 Comparing Freezing and Anisotropy

As already mentioned, anisotropic magnets differ from isotropic magnets by having a preferred direction of magnetization, i.e., there is a direction in which the magnet can be easier magnetized. Since there already exist simulations for anisotropic magnets where all parameters are known, it would be interesting to know whether one can describe the simulation of an isotropic magnet including the freezing condition via a simulation of anisotropic magnets (see Figure 13).

To find out whether this is possible or not, comparisons of the simulation including the freezing condition with simulation of a magnet with anisotropic material law were done.

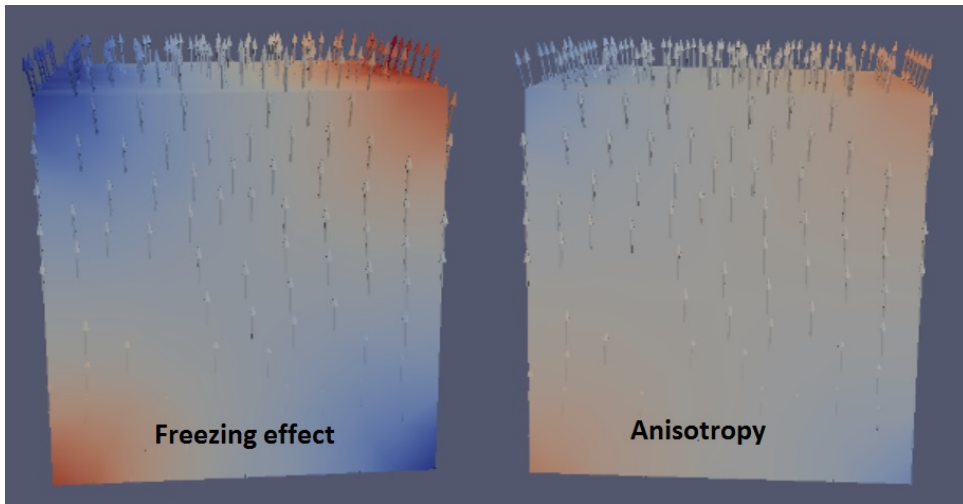


Figure 13: Magnetization of FEMME simulation of isotropic magnet with freezing condition and FEMME simulation of anisotropic magnet plotted with Paraview. (Left) The magnetization of the simulation including the freezing condition clearly shows flower state. (Right) Simulation of anisotropic magnet shows slight tendency of flower state, but not as clearly as for freezing simulation. Differences in the magnetization between the two simulations can be seen by the colors which indicate the magnetization.

3.1 Choice of Parameters

It is characteristic for isotropic magnets that the major loops look the same no matter in what direction the magnetization is saturated. This is since the susceptibility χ and thus also the permeability μ are both scalar.

In contrast to this, for magnets with uniaxial anisotropy [27], the direction in which the magnetization is saturated determines the shape of the hysteresis curve. [28] The susceptibility χ and also the permeability μ get 3×3 tensors in this case.

This tensor can be diagonalized and reads then as

$$\underline{\mu} = \begin{pmatrix} \mu_x & 0 & 0 \\ 0 & \mu_y & 0 \\ 0 & 0 & \mu_z \end{pmatrix} \quad (3.1)$$

With an anisotropic material law given by [2] $\mathbf{M} = \mathbf{M}_r + \underline{\chi}\mathbf{H}$, the equations describing the material with a reduced scalar potential are

$$\mathbf{H} = \mathbf{H}_{\text{ext}} - \nabla u \quad (3.2)$$

$$\nabla \cdot (\underline{\mu}^+ \nabla u^+) = \nabla \cdot (\underline{\mu}^+ \mathbf{H}_{\text{ext}} + \mathbf{M}_r) \quad (3.3)$$

$$\nabla^2 u^- = 0 \quad (3.4)$$

$$u^+ - u^- = 0 \quad (3.5)$$

$$\nabla u^+ \cdot \underline{\mu} \cdot \mathbf{n} - \mu^- \frac{\partial u^-}{\partial n} = \mathbf{n} \cdot \underline{\chi} \cdot \mathbf{H}_{\text{ext}} + \mathbf{n} \cdot \mathbf{M}_r \quad (3.6)$$

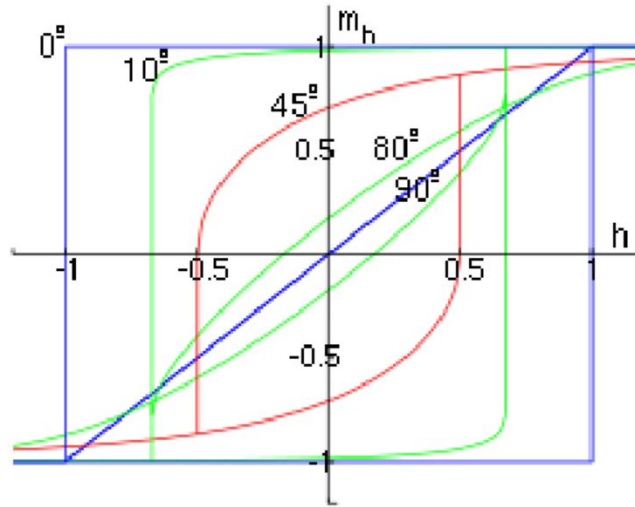


Figure 14: Different shapes of ideal hysteresis loops of magnet with uniaxial anisotropy and different angles ϕ respective to the easy axis. As the angle ϕ approaches 90° the loops become slimmer and finally become a single line when the direction of the field is perpendicular to the easy axis. ¹⁴

If the magnet is saturated in the direction of the easy axis, the shape of the hysteresis curve is different to the shape of the hysteresis curve when fields at arbitrary angles ϕ

¹⁴Image taken from Wikimedia Commons: https://commons.wikimedia.org/wiki/File:SwHyst_vs_angle.svg

to the easy axis are applied. In particular the loops become thinner as ϕ approaches 90° . Particularly, if the external field is applied in the direction of the hard axis, i.e., the axis perpendicular to the easy axis, the ideal hysteresis loop becomes a straight line as seen in Figure 14. In Figure 15 this behavior can also be seen in measurement data of a hard magnet.

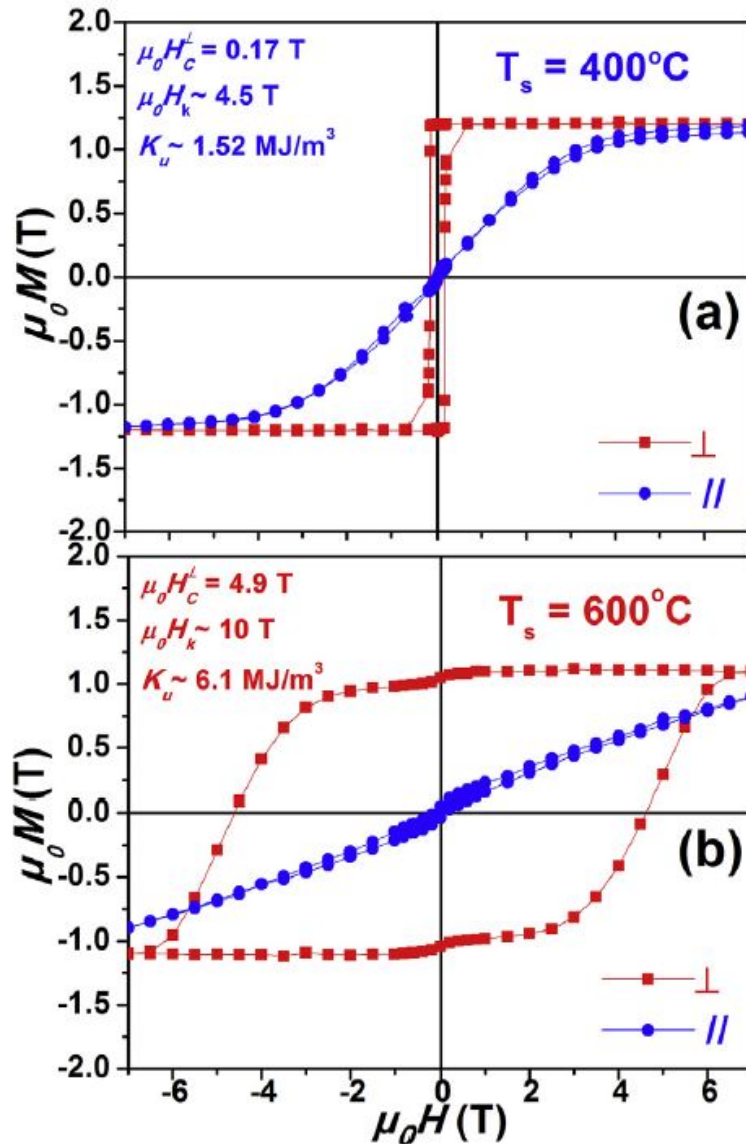


Figure 15: Measurement of magnetic hysteresis of (a) single 9.5nm semi-hard FePt film deposition MgO (001) at 400°C and (b) single 9.5nm $L1_0$ FePt-C film deposited on MgO (001) at 600° . Hysteresis when the field is applied in the direction of easy axis (red) and in direction of hard axis (blue) showing different behavior as described above. ¹⁵

¹⁵Image taken [26].

In this comparison a pure anisotropic magnet model is compared with a model of an isotropic magnet including the freezing condition. The field is applied in z-direction. The susceptibility of the isotropic magnet χ as well as the longitudinal susceptibility χ_z is assumed to be the same.

Note that this assumption is not true in reality. In fact it seems like anisotropy and field freezing both have a contribution and it is hard to distinguish them.

During all simulations of magnets with an anisotropic material law in this chapter, the longitudinal permeability μ_z is assumed to be constant, i.e., $\mu_z = 1 + \chi_l = 1.15$. The transversal susceptibility χ_t is to be varied. The question is, whether it is possible to simulate an isotropic magnet with freezing effect with the help of an anisotropic material law with the correct choice of χ_t , or not.

All simulations were done with FEMME. The shape used in the simulation is a simple cube with dimensions 5mm×5mm×5mm.

The first question that appears is how to choose the transversal susceptibility χ_t and the freezing field H_{freeze} in the comparison, in order to get the same effect - if this is possible.

To find the correct choice of this two parameters, the quadratic average magnetization of one component in both simulations was compared. The quadratic average magnetization in one component is computed in the following way.

$$\langle M_i^2 \rangle = \sum_{n=1}^N \frac{\mathbf{m}_{n,i}}{N} \quad i = x, y, z \quad (3.7)$$

where N is the number of elements used in the simulation. H_{freeze} and χ_t are chosen in such a way that the quadratic average magnetization is equal in one component. Then it is checked whether the quadratic average magnetization in the other components matches or not.

If the quadratic average magnetization is the same for all components for the same H_{freeze} and χ_t , then both simulations describe the same effect.

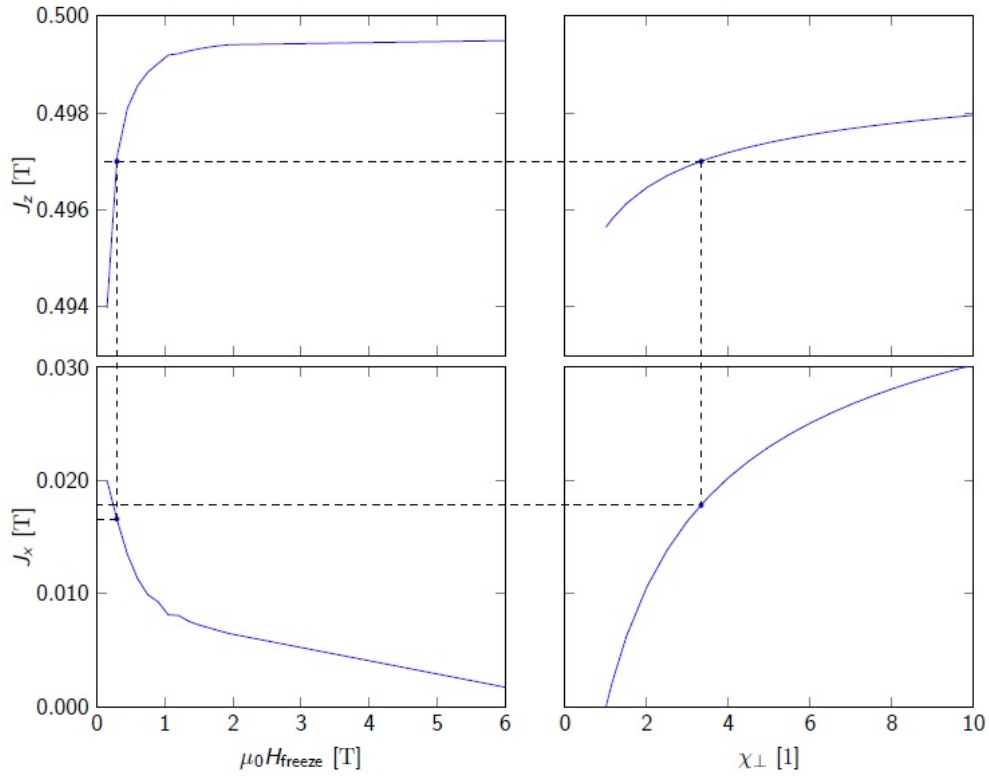


Figure 16: Choosing H_{freeze} and χ_t such that the quadratic average magnetization is the same for the z-component. With these parameters the quadratic average magnetization in the x-component is then checked, showing that it is different in both cases.

As it can be seen in Figure 16, if the quadratic average magnetization for the z-component is matched, the quadratic average magnetization in the x-component for the same H_{freeze} and χ_t shows significant difference. This graphic already indicates that it is not possible to describe field freezing via an anisotropic material law.

3.2 Deviation between Freezing and Anisotropy

To investigate the deviation between anisotropy and freezing more clearly, a value to indicate the deviation between the simulation including the freezing condition and the simulation of an anisotropic magnet is computed. Additionally, the deviation is made visible in different plots.

3.2.1 Deviation Measure

To compute the value indicating the deviation for every component, the following objects are needed.

- \mathbf{m}_0 ... resulting magnetization vector of simulation of isotropic magnet without the freezing condition
- \mathbf{m}_{freeze} ... resulting magnetization vector of simulation of isotropic magnet including the freezing condition.
- \mathbf{m}_{ani} ... resulting magnetization vector of simulation of an anisotropic magnet.

The componentwise difference of the freezing and the anisotropy simulation to the isotropic magnet is then calculated:

$$\mathbf{m}_{0,i} - \mathbf{m}_{freeze,i} \quad \text{and} \quad \mathbf{m}_{i,0} - \mathbf{m}_{ani,i} \quad i = x, y, z \quad (3.8)$$

This computation gives two vectors for each component. They express the deviation of the simulation including the freezing condition and the simulation with anisotropic material law to the simulation of the isotropic magnet without the freezing condition. For each component these two vectors are normalized and the scalar product of the normalized difference vectors is built. The absolute value of the scalar product lies between 0 and 1 and indicates the difference between the freezing effect and anisotropy. In particular,

$$\frac{\mathbf{m}_{0,i} - \mathbf{m}_{freeze,i}}{\|\mathbf{m}_{0,i} - \mathbf{m}_{freeze,i}\|} \cdot \frac{\mathbf{m}_{0,i} - \mathbf{m}_{ani,i}}{\|\mathbf{m}_{0,i} - \mathbf{m}_{ani,i}\|} \in [0, 1] \quad i = x, y, z \quad (3.9)$$

If the value is close to 1, that means that both effects are similar or equal in the corresponding component. If the value is away from 1 the effects are different from each other.

As an example for this calculation, a cube with dimensions 5mm×5mm×5mm is considered. The field is applied in z-direction. The susceptibility in the freezing model is $\chi = 0.15$. H_{freeze} and χ_t are chosen such that the x-component of the average magnetization matches for both effects. In this example $\mu_0 H_{freeze} = 0.6\text{T}$ and $\chi_x = 1.0$, i.e., $\mu_x = 2.0$. Now the difference vectors $\mathbf{m}_{0,x} - \mathbf{m}_{freeze,x}$ and $\mathbf{m}_{0,x} - \mathbf{m}_{ani,x}$ for the x-component are built and the scalar product of the normalized difference vectors is computed. The value of the scalar product in this case is 0.99999, i.e., almost 1. This is

clear, since the parameters were chosen in order to get this result. Moreover, the repetition of this procedure for the y-component, i.e. $\chi_y = 1.0$ yields almost the same value, i.e., a value which is close to 1. Thus, if the x-component of the average magnetization is matched, additionally an accordance in the y-component is achieved. However, the computation of the value for the z-component with $\chi_z = 0.15$ gives a value of 0.676547, which implies that there is some difference between the two effects in the z-component.

3.2.2 Visualization of Deviation

In fact, if the computed difference of the simulation including the freezing condition and the simulation of an anisotropic magnet is plotted, like in Figure 17 and Figure 18 the variation of the two effects can be seen.

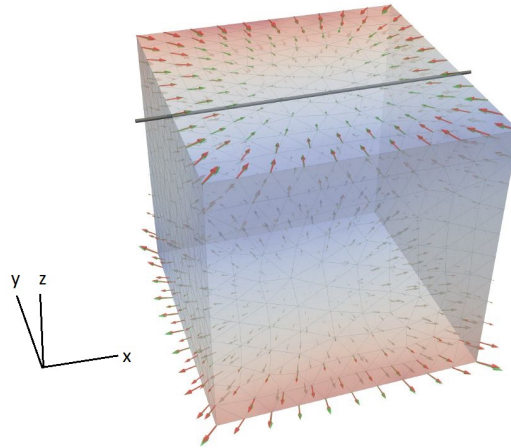


Figure 17: Difference of magnetization vectors of simulation including the freezing condition (green) and simulation of anisotropic magnet (red).

In Figure 18 it can be seen that the quadratic average magnetization of both simulations in the x-component is equal, which implies that both effects are the same in the x-component.

In the z-component it is visible that the quadratic average magnetization is significantly different, which was already indicated by the value deviating from 1. While there is no difference in the z-component between the isotropic magnet and the anisotropic magnet, an obvious deviation between the difference of the isotropic magnet without and with the freezing effect is recognizable. The drift that can be seen here indicates that the freezing effect takes the rotation of the magnetization vectors into account and describes the flower state of the remanence magnetization. However, the simulation of a magnet with anisotropic material law only changes the transversal magnetization, since

only χ_t has been changed. This leads to a slight rotation, but also a scaling of the magnetization vector.

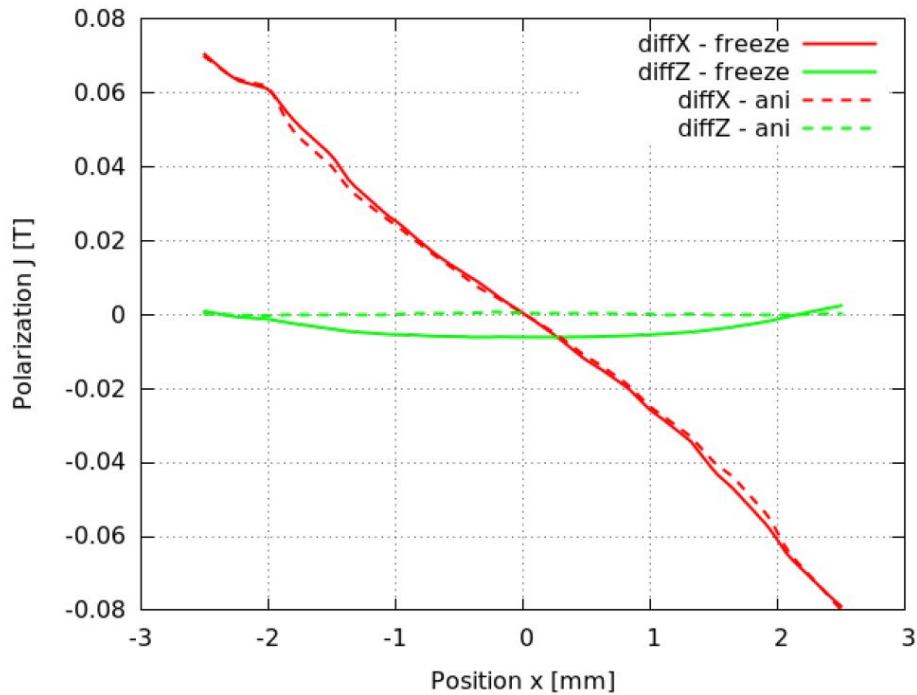


Figure 18: Difference in x-component (red) and z-component (green) of magnetization between difference vectors $\mathbf{m}_0 - \mathbf{m}_{freeze}$ and $\mathbf{m}_0 - \mathbf{m}_{ani}$. The x-component of the magnetization matches for both simulations. However, the magnetization of the z-component shows a significant difference between the effects. The drift of the difference vector of the simulation including the freezing condition indicates that the freezing model considers the rotation of magnetization vectors, whereas the simulation of an anisotropic magnet only changes the magnitude of magnetization vectors.

In summary this shows, that the freezing effect of an isotropic magnet and an anisotropic magnet are different from each other and it is not possible to describe the freezing effect by an anisotropic material law.

4 Computer Experiment to Determine H_{freeze}

The idea of this section is to find the freezing field H_{freeze} via a computer experiment as suggested by Udo Ausserlechner from our cooperation partner Infineon. For the simulations of the computer experiment a Stoner - Wohlfarth model is used.

Stoner-Wohlfarth models have been already explained in Section 2. The setting and the results of the computer experiment are explained in this section.

The simulations were performed using magnum.fd, a micromagnetic simulation code based on a finite-difference approximation. Material parameter of NdFeB were used to simulate the Stoner-Wohlfarth particles. 30^3 cells were used for the simulations of the rotation about 90° and the number of steps to rotate and decrease the field is 300. In the simulations of the rotation about 180° the number of steps is 600.

4.1 Stoner - Wohlfarth Model: Setting

The setting of the computer experiment is the following.

A magnet which consists of non-interacting Stoner - Wohlfarth particles is considered. The orientation of the easy axes of the particles is assumed to be distributed randomly. The particles are simulated with the micromagnetic code magnum.fd (forked from MicroMagnum [30]). To simulate the magnet with a micromagnetic code the exchange interaction constant A is set zero. Additionally, no demagnetizing field is considered. Thus, the shape of the magnet has no influence on the simulation.

To find the energy minimum, the algorithm uses time integration of the LLG equation and relaxing into a stable state.

An external field $\mu_0 H_{ext}$ in z -direction is applied. The magnitude of the external field is chosen such that the magnetization vectors of the magnetic grains are aligned in the direction of the external field, i.e., the magnetization of the grains should be aligned in z - direction (see Figure 19). Thus, the external field has to be larger than the anisotropy field of the grains. During the whole experiment only the average magnetization of the magnet is considered.

The intention of this computer experiment is to find boundaries for the freezing field.

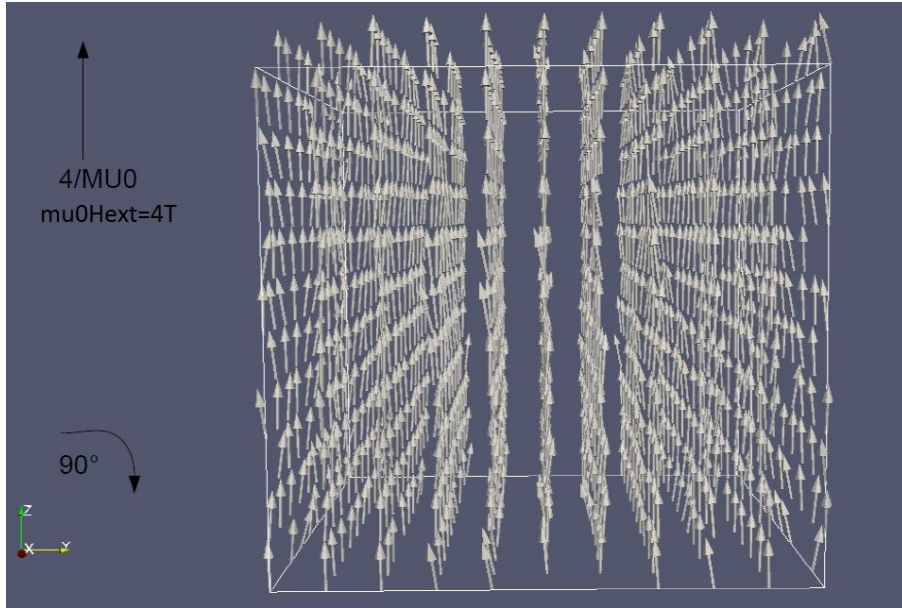


Figure 19: Resulting magnetization due to applied field in z-direction of magnitude $\mu_0 H_{ext} = 4\text{T}$. The magnetization vectors are aligned in the direction of the applied field.

The field is now rotated about 90° in steps of uniform size and simultaneously the amplitude of the external field is reduced to zero in the same amount of steps. Another computation, where the external field is rotated about 180° , is done in a second step. For the rotation about 180° , twice the amount of the steps in the simulation of the rotation about 90° were used.

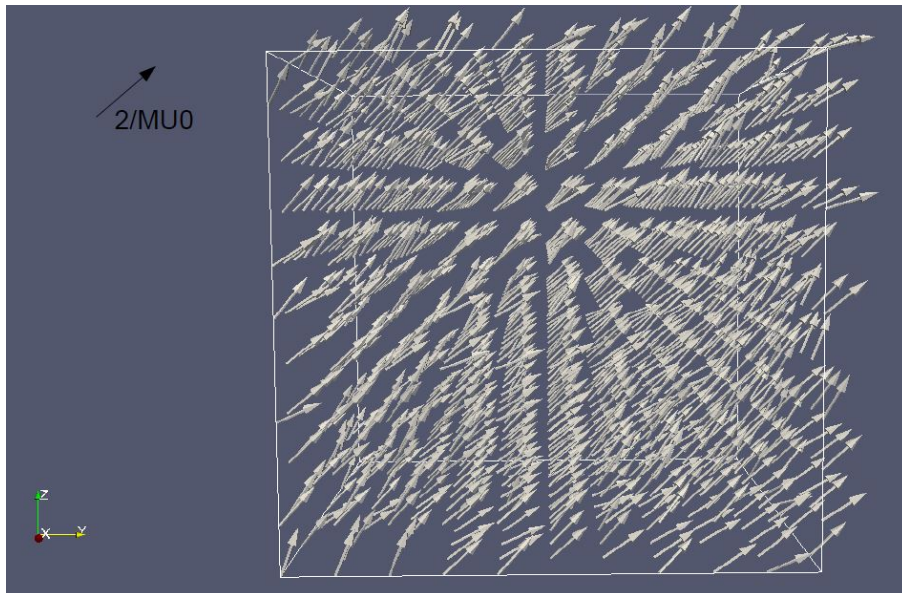


Figure 20: Resulting magnetization after a rotation about 45° and a decreased field $\mu_0 H_{ext} = 2\text{T}$. Nearly all magnetization vectors are aligned in the direction of the applied field.

As it can be seen in Figure 20, after a rotation about 45° and the reduction of the applied field by half, the magnetization vectors are nearly perfectly orientated in the direction of the applied field, showing that the field is still bigger than the freezing field.

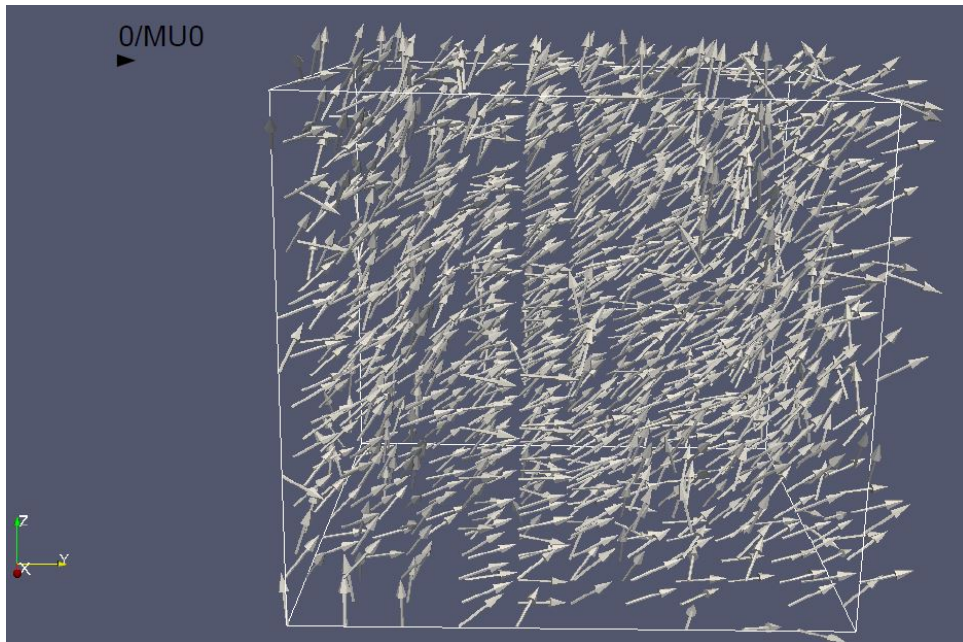


Figure 21: Resulting magnetization after applied field is turned off. The magnetization vectors are no longer aligned in the same direction, indicating that there is a threshold where the applied field gets too small to align the magnetization vectors.

In Figure 21 it can be seen that if the external field is turned off the magnetization vectors are no longer perfectly aligned. Thus, at some point the applied field gets too small to align the magnetization vectors in the direction of the field. This critical field is the searched freezing field H_{freeze} .

After the external field is turned off, the angle of the average magnetization is calculated. The amplitude of the field that was applied at this angle is the searched H_{freeze} . This approach can be seen in Figure 22.

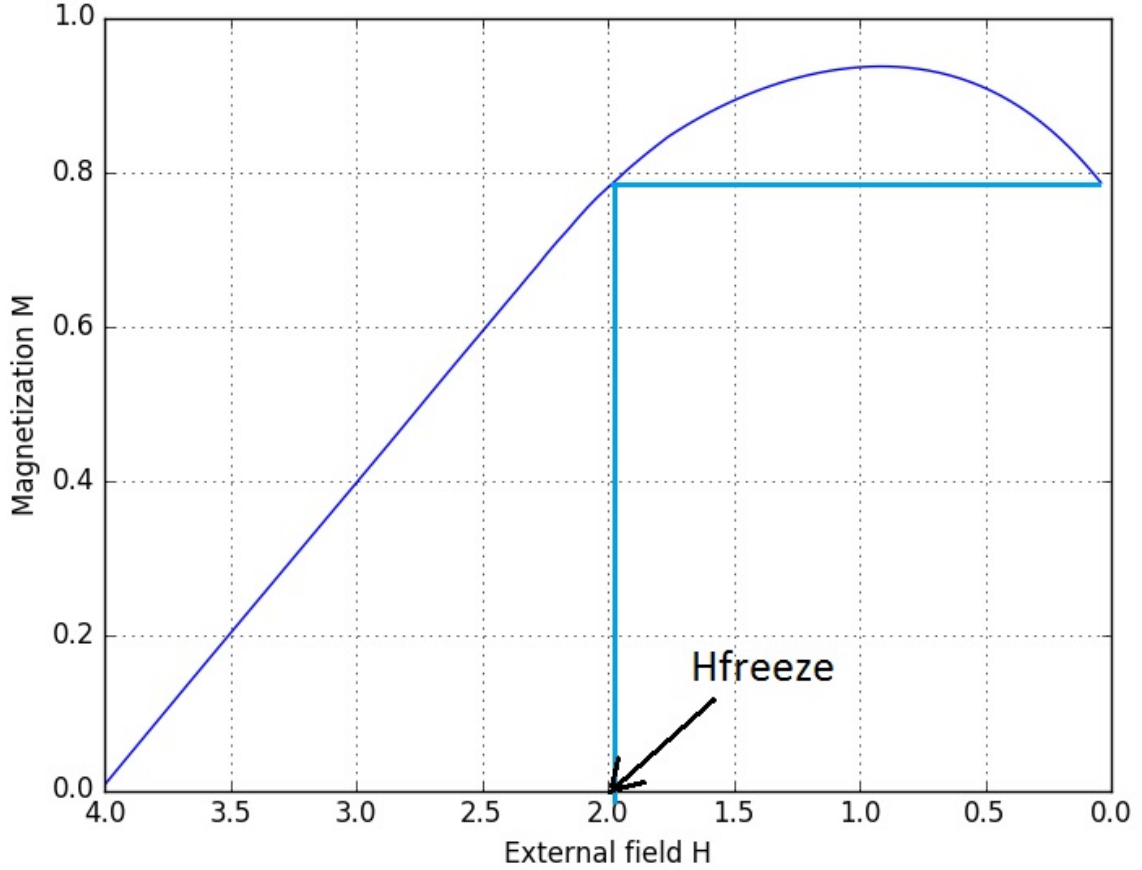


Figure 22: Strategy to find H_{freeze} . The amplitude of the field that was applied at the angle of the average magnetization if the external field is turned off is the searched H_{freeze} .

One interesting question here is whether the computed freezing field H_{freeze} coincides with the obtained freezing field from the comparison of simulation and the measurement later in this work when the correct material parameters are chosen. The other interesting question is, whether the rotates about 90° and about 180° lead to the same result and if the ratio H_{freeze}/H_k is independent of the special choice of the material.

4.2 Material Parameter

First, it is necessary to determine the material parameters that are used for the computation with magnum.fd.

The material that is simulated is NdFeB, a permanent magnet made from an alloy of neodymium, iron and boron. It is the most widely used rare earth magnet and the strongest type of permanent magnet that is commercially available.

The material parameters for the simulation of NdFeB read as

- $J_s = 1.63\text{T}$
- $K_1 = 4.3 \cdot 10^6 \frac{\text{J}}{\text{m}^3}$

where J_s denotes the saturation magnetization and K_1 is the uniaxial anisotropy constant.

With this material parameters, the anisotropy field H_k [5] is

$$\mu_0 H_k = \frac{2K}{J_s} = 6.63\text{T} \quad (4.1)$$

For the Stoner - Wohlfarth model the relation $H_c = H_k = 6.63$ is assumed if the field is applied in the direction of the prescribed easy axis.

Assuming these parameters, it suffices to chose an initial applied field bigger than H_k , for example $\mu_0 H_{ext} = 7.0\text{T}$.

4.3 Results

Comparing the results from the computer experiment with the rotation about 90° and the one about 180° in Figure 23 shows that for the assumed material parameters the freezing - field is not independent of the size of the rotation. The rotation about 90° leads to a higher freezing field than a rotation about 180° as can be seen in Table 1. Note that every field value was relaxed into a stable state.

Rotation about	$\mu_0 H_{freeze}$	H_{freeze}/H_k
90°	5.25T	0.79
180°	4.6T	0.69

Table 1: Results of the computer experiment showing that the rotation about 90° and 180° do not lead to the same freezing field.

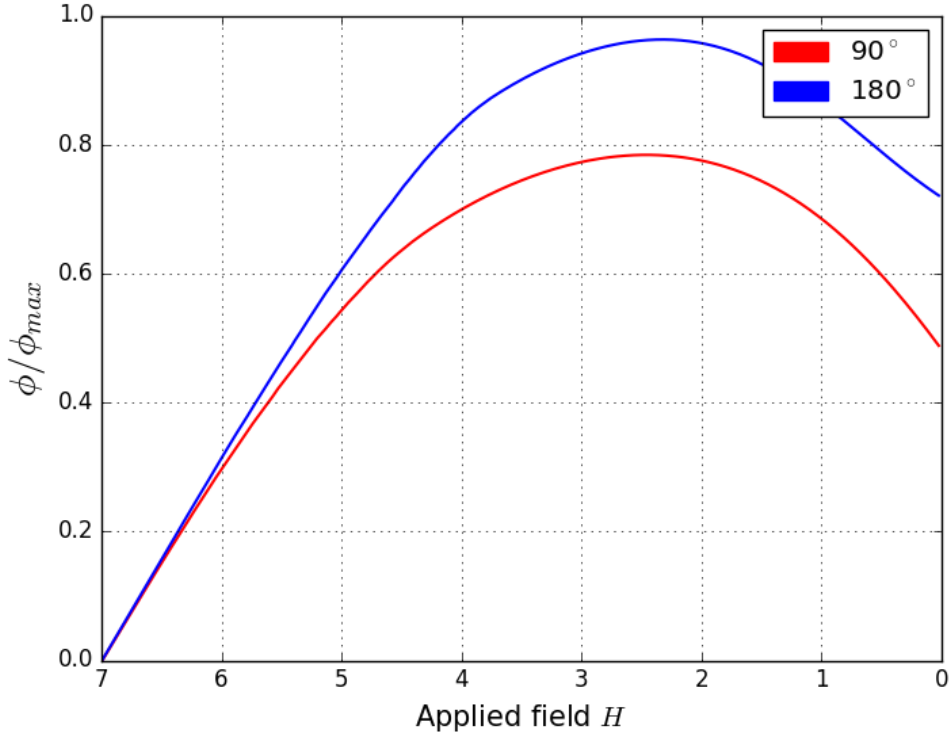


Figure 23: Angle of average magnetization over applied field, rotation about 90° and 180° showing that the resulting freezing field is not independent of the size of the rotation.

The computer experiment was repeated with different material parameters. The results are similar to the ones for NdFeB, also giving a higher freezing field for the rotation about 90° than for the rotation about 180°. The ratio between H_{freeze}^{90} and H_{freeze}^{180} to H_k is also almost the same as in the former computations. This indicates that the freezing field depends indeed on the size of the rotation but the ratio of the freezing field to the anisotropy field is independent of the material.

Comparing the freezing fields of the computer experiment with the freezing field that is computed by comparing the simulations to the measurement shows, that the freezing field computed by the computer experiment is much bigger than the freezing field that comes from the measurements.

The results of the computer experiment are not as expected. It seems that a simple Stoner-Wohlfarth model is not appropriate for the experiment. It was expected that the rotation about 90° and 180° do not give different freezing fields. Thus the results of the computer experiment are quite surprising. However, boundaries for the freezing field in dependence of the anisotropy field can be seen from the computer experiment.

4.4 Extended Stoner - Wohlfarth model: Computing H_k and H_c

Since the computed H_c in the computer experiment is much higher than the measured one, the question arises whether the simulation of the computer experiment can be improved or not.

The problem with the usual Stoner - Wohlfarth model is that the ratio $H_c = H_k$ is not correct in real life and thus leads to a too high coercivity field H_c . This is known as Brown's paradox.[29]

Target of this section is to compute the correct ratio between H_k and the intrinsic H_{ci} with the help of the so called "devicemodel" [31], a model that is used to simulate GMR sensors in a rotating field. The devicemodel is based on the extended Stoner-Wohlfarth model, where the h_y -field is scaled. It should be noted that the devicemodel is a 2D-model and thus not really what is needed for the computations in this work. However, to compute the ration between H_k and the intrinsic H_{ci} , the model is sufficient.

As already mentioned the correct ratio between H_k and H_c should be found in order to improve the simulations. To achieve this, it is necessary to differentiate between the extrinsic coercivity field H_c , which characterizes the coercivity of the whole magnet, and the intrinsic coercivity field H_{ci} . [8] This intrinsic H_{ci} describes the coercivity of one particle. Since the devicemodel iteratively solves a Stoner - Wohlfarth model, the intrinsic H_{ci} is needed.

By the use of hysteresis matching, the accurate H_{ci} is evaluated. The parameters that are fitted by the computation of a hysteresis loop are the measured initial susceptibility $\chi = 0.167$ and the measured external coercivity field $\mu_0 H_c = 1.13\text{T}$. The susceptibility χ_t is visible as the slope of the initial minor loop of the hysteresis curve. H_{ci} can be seen from the hysteresis curve as the applied field at which the magnet is fully demagnetized again, i.e., the field at which the hysteresis loop crosses the x-axis.

The variables that can be changed during the computation are the ratio between H_{ci} and H_k and the angle of the easy axis ϕ . Since the model is only 2D the easy axes of the particles are uniformly distributed in the plane.

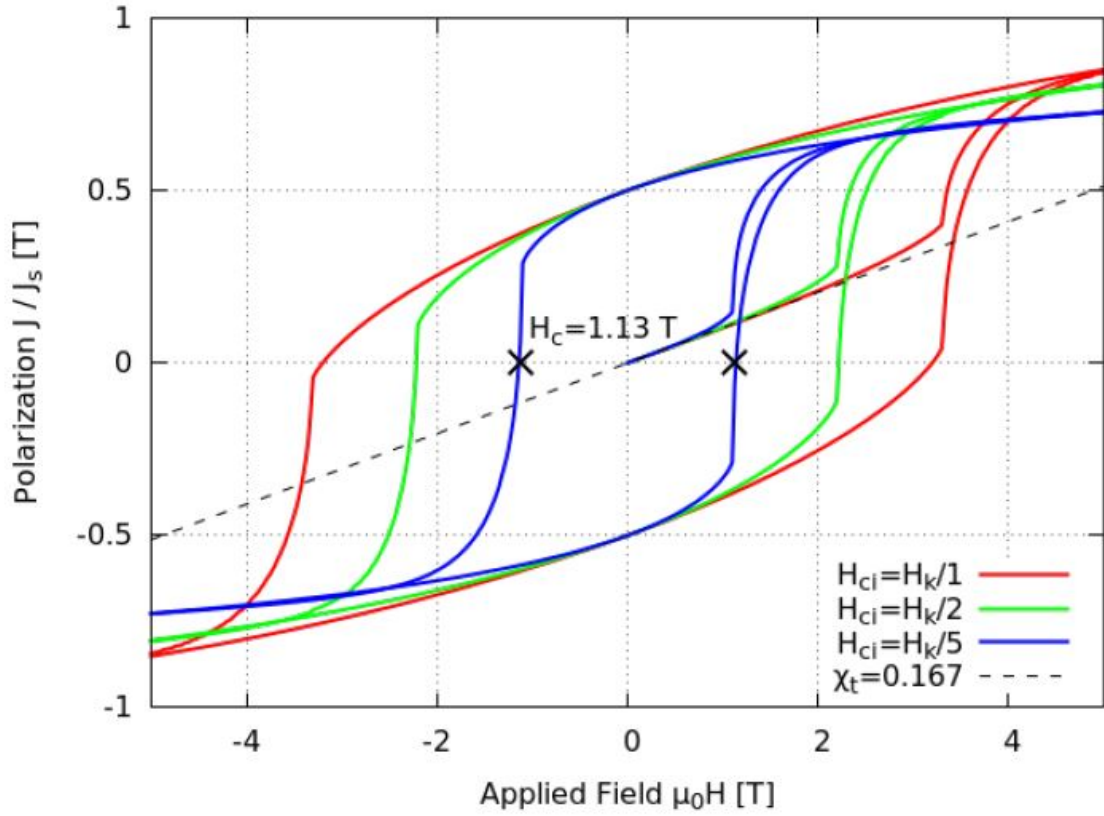


Figure 24: Hysteresis matching

The major loop in Figure 24 plot shows that for the computed $\mu_0 H_k = \frac{2K}{J_s} = 6.63$ T the measured transversal susceptibility χ_t is correct.

The next step is to find the ratio $\frac{H_k}{H_{ci}}$ such that H_c is correct. Different ratios have been tested, among other things the ratio that is used in the Stoner - Wohlfarth model. It can be seen that for

$$H_{ci} = \frac{H_k}{5} \quad (4.2)$$

the measured H_c is correct.

5 Comparing Measurement and Simulation

To validate the simulations of the freezing effect and adjust the needed parameters of the simulations, measurements with different geometries were done. Additionally, the question whether different materials and different geometries have different freezing field H_{freeze} will be answered.

5.1 Measurement

The Magnetfabrik Bonn produced isotropic magnets in two geometries and three different materials. The geometries that were chosen for the measurement are on one hand a simple cube and on the other hand an L-Shape. The dimensions of the geometries can be seen from Figure 25. Both geometries are such that their negative part is the geometry itself.

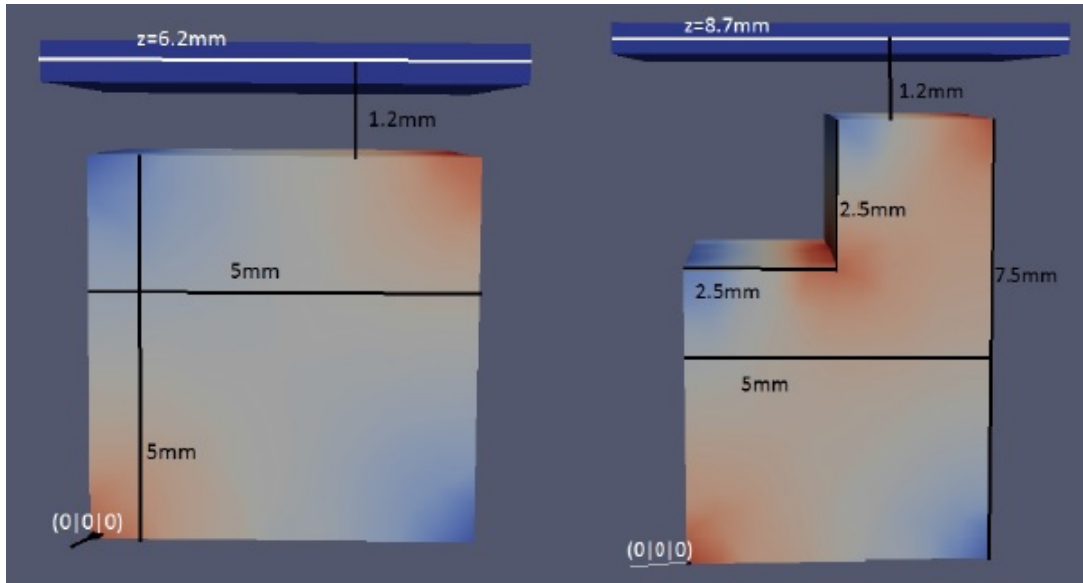


Figure 25: Geometry proposal for magnets produced and measured by MF Bonn. The dimensions of the cube are 5mm x 3.2mm x 5mm. The total dimension of the L-Shape is 7.5mm x 3.2mm x 5mm and the dimension of the notch is 2.5mm x 3.2mm x 5mm.

The materials that were used for the production of the magnets are neofer_25_60p, neofer_40_100p and neofer_48_60p. All these materials are composed of NdFeB and the polyamide PA11. They differ by having various remanent magnetizations and different coercivities.

The most important material parameters of the three materials can be seen in the following Table 2.

Material	\mathbf{B}_r [mT]	\mathbf{H}_{cB} [$\frac{\text{kA}}{\text{m}}$]	\mathbf{H}_{cJ} [$\frac{\text{kA}}{\text{m}}$]	$(\mathbf{BH})_{max}$ [$\frac{\text{J}}{\text{m}^3}$]	$\chi = \frac{\mathbf{B}_r}{\mu_0 \mathbf{H}_{cB}}$
neofer_25_60p	400	260	630	27	0.22
neofer_40_100p	460	310	1000	36	0.18
neofer_48_60p	540	330	600	48	0.3

Table 2: Important material parameters of neofer_25_60p, neofer_40_100p and neofer_48_60p taken from the data sheets of Magnetfabrik Bonn.

The measurements were done in the following way:

First, the magnet and its negative part were magnetized together in z-direction. Then, the negative part was removed and the magnetic field was measured in a distance of 1.2mm and 2.5mm above the upper surface of the magnet (see Figure 26). From this measurement one gets data that is to be compared with the simulations of an isotropic magnet without the freezing condition.

Then, the magnet was demagnetized as good as possible. In the next step the magnet was magnetized again in z-direction but this time without the negative part. This measurement resembles the simulation including the freezing condition. Finally, the magnetic field was again measured in the same distances as before.

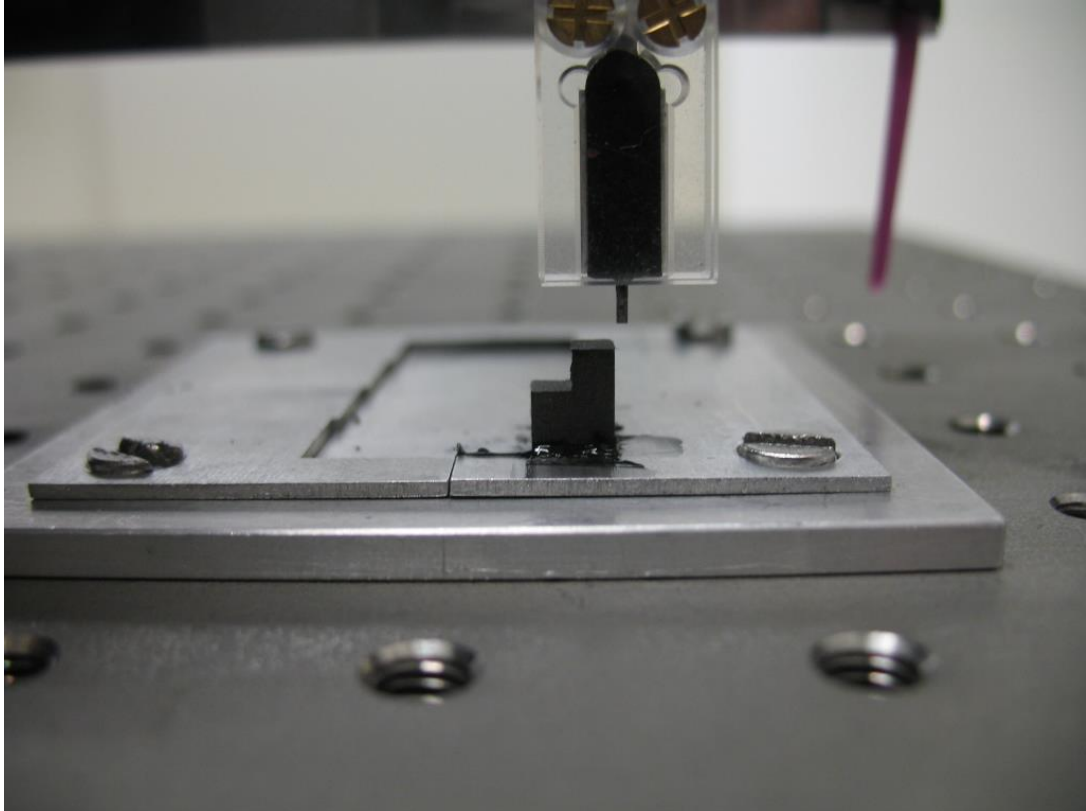


Figure 26: Measurement of neofer_25_60p L-Shape with 3D probe hall sensor by Infineon Austria.

5.2 Comparison

The measurement data of MF Bonn are compared with simulations. The procedure is the same for all materials and both geometries.

Step 1 is to compare the measurement with and without the negative part and see how big the difference between the measurements is. From this comparison it can be seen whether there is a misalignment of one measurement or not. If the peaks of both measurements are not one above the other, this indicates a misalignment in the measurement, since the simulations only show a shift in vertical direction but not in horizontal direction.

The next step is to fit the simulation of the isotropic magnet without the freezing effect to the measurement with the negative part. This is done by varying \mathbf{B}_r and the permeability μ in order to get the best match, i.e., the smallest deviation between the data.

With these two parameters fixed, the simulation including the freezing effect is compared to the data of the measurement without the negative part. By comparing simulations with different H_{freeze} to the measurement data, the freezing field is determined in order to get the best match between simulation and measurement.

As an example, the comparison between the simulation and the measurement for the L-Shape of material neofer_25_60p in 1.2mm distance is done step by step. The results of the other comparisons are summarized after this detailed explanation.

5.2.1 Simulations

The first thing to consider, is the comparison of the simulations without the freezing effect and including it.

The plot in Figure 27 shows that the difference between the freezing - and the nonfreezing-simulation is, as already mentioned before, a shift of the peak only in vertical direction. Indeed, also in the comparison between the simulations for the L-Shape, the shift is only in z-direction. Thus, if there is a shift of the data in x-direction, this may indicate a misalignment at the measurement or other errors during the measurement.

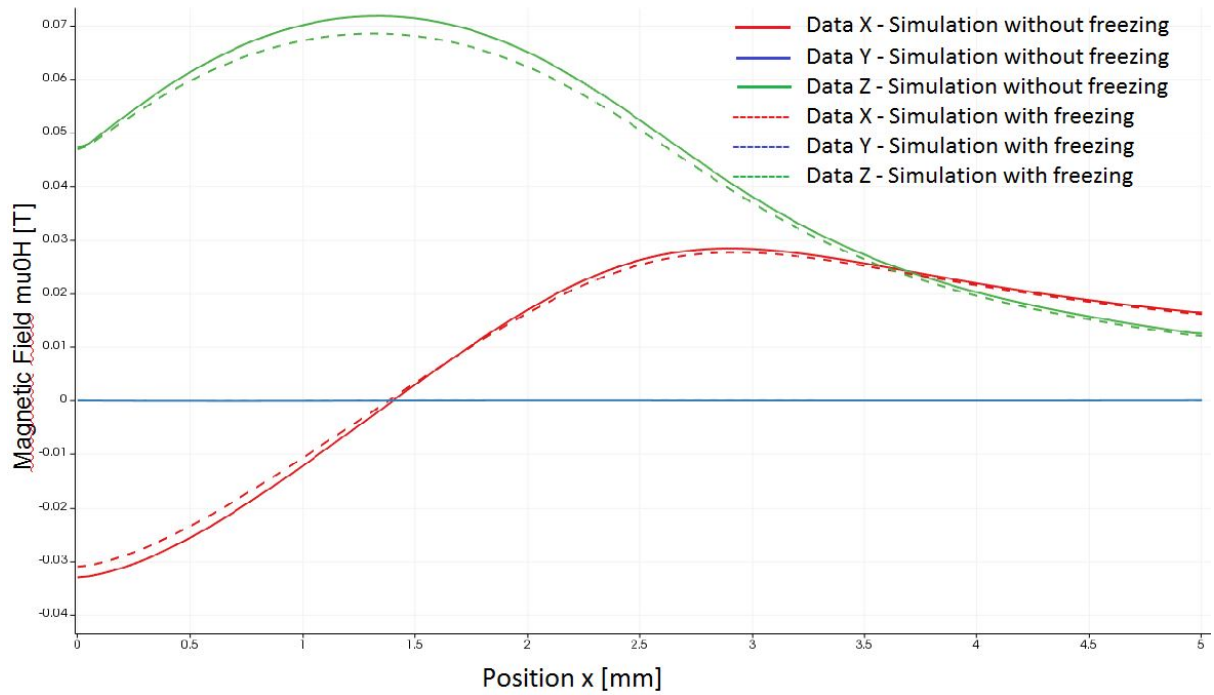


Figure 27: Comparison of L-Shape-simulations of isotropic magnet without the freezing condition and including the freezing condition, showing that the shift between plots is only in vertical direction.

5.2.2 Measurement

The comparison between the measurement with negative part and the one without negative part shows that the deviation between the two measurements is not only in vertical direction but there is also a small shift of the data in horizontal direction (see Figure 28).

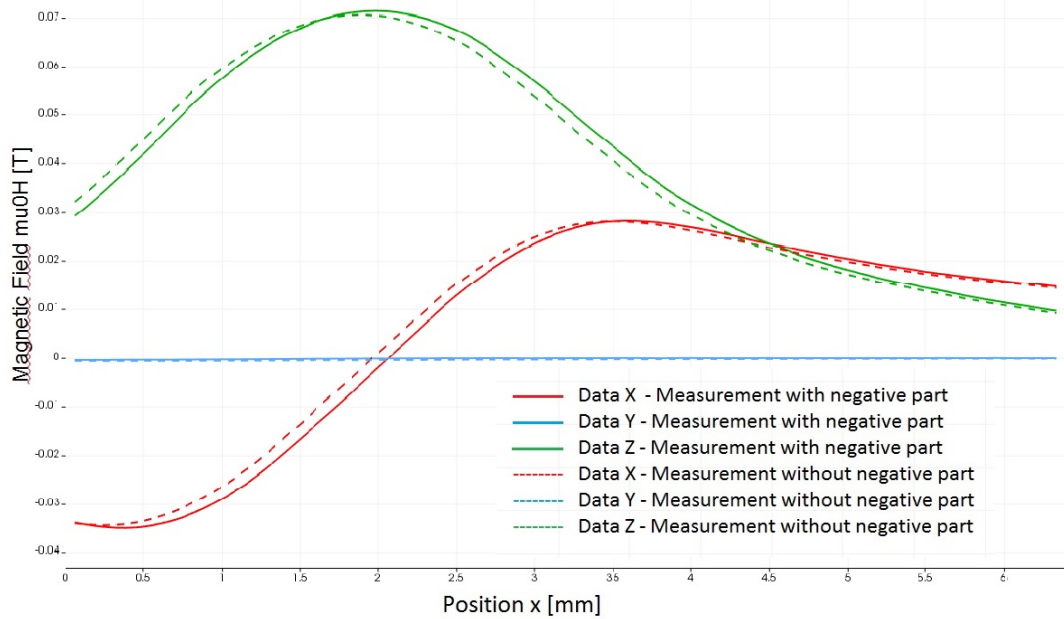


Figure 28: Comparison of neofer_25_60p L-shape measurement data with and without negative part, showing a shift between the data in x-direction. The shift indicates a misalignment in the measurement, but this can be verified with the help of a measurement rotated about 180° and taking the average of it.

Shifting the data of the measurement without the negative part in x-direction by 0.322mm gives only a shift in vertical direction as seen in Figure 29 just as in the simulations.

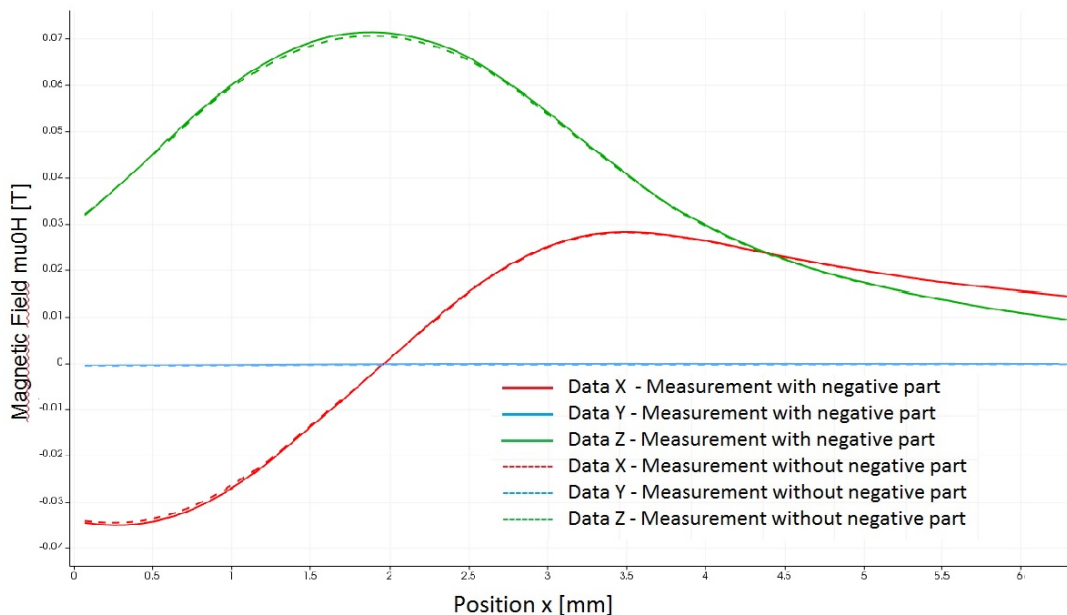


Figure 29: Comparison of shifted neofer_25_60p L-shape measurement data with and without negative part.

5.2.3 Measurement with Negative Part vs. Non-freezing Simulation

The next step is to adjust \mathbf{B}_r and μ such that the data of the measurement with negative part and the simulation without the freezing effect correspond with each other. This is done the following way: Simulations with different parameters are compared to the measurement and the sum of maximal distances between the points is computed and minimized. The parameters of the simulation that fits best are chosen. In the case of the neofer_25_60p-Cube the parameters that fit best are $\mathbf{B}_r = 360\text{mT}$ and $\mu = 1.07$ (see Figure 30). The deviation of the fitted \mathbf{B}_r from the value in the data sheet can result from temperature, surface properties or measurement errors.

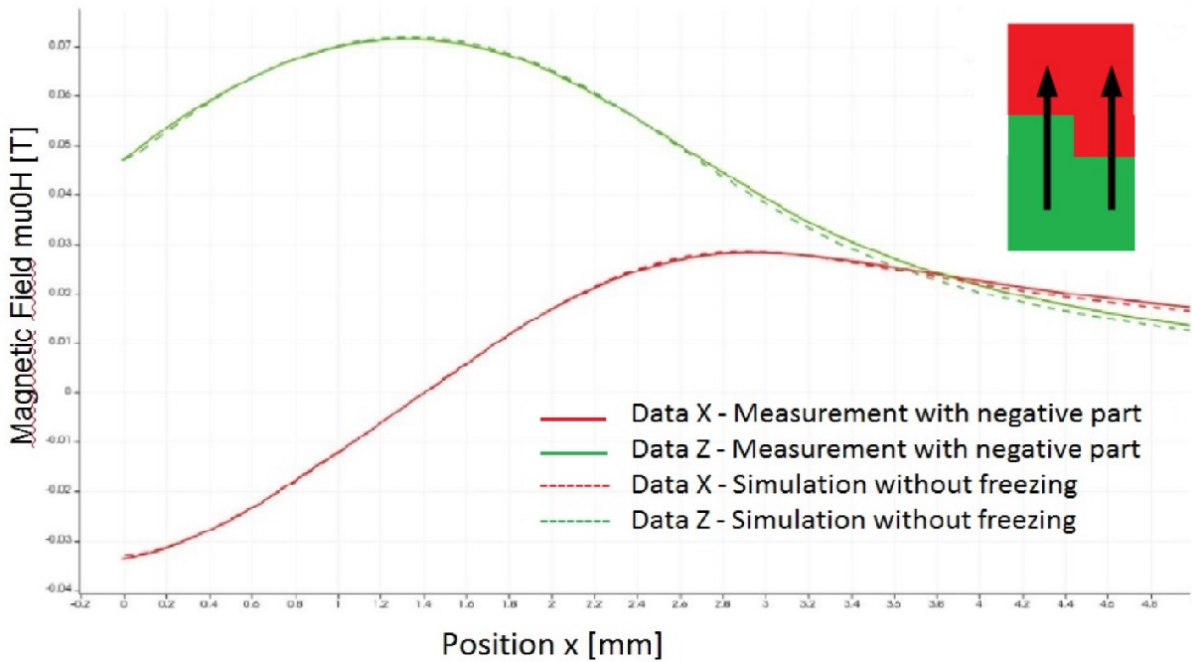


Figure 30: Simulation of L-Shape without the freezing condition fitted to neofer_25_60p L-shape measurement with negative part. Parameters, for which measurement and simulation fit best, are $\mathbf{B}_r = 370\text{mT}$ and $\mu = 1.15$

5.2.4 Measurement without Negative Part vs. Freezing Simulation

With the chosen parameters the goal is to find the freezing field for the given material and the given shape. For that purpose, simulations with different freezing fields are done and compared to the data of the measurement without the negative part. The freezing field of the simulations, that fits best to the measurement data, is the chosen H_{freeze} .

Figure 31 shows the comparison of the measurement without the negative part with freezing simulations with two different H_{freeze} . The freezing fields are $H_{freeze1} = 0.6\text{T}$ and $H_{freeze2} = 3.5\text{T}$. From the comparison it is visible that the simulation with

$H_{freeze} = 3.5\text{T}$ agrees with the measurement data.

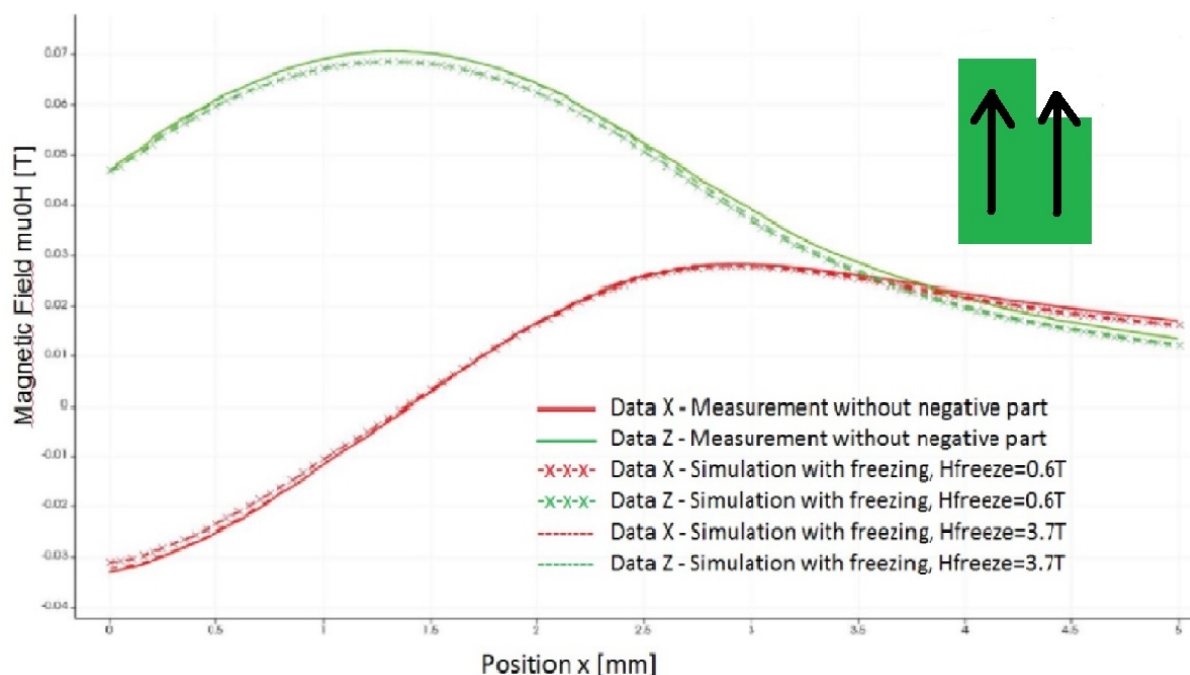


Figure 31: Simulation of L-shape including freezing condition fitted to neofer_25_60p L-shape measurement with negative part. Tested freezing fields are $H_{freeze1} = 0.6\text{T}$ and $H_{freeze2} = 3.5\text{T}$. The simulation with $H_{freeze2} = 3.5\text{T}$ fits the measurement data best.

5.2.5 Results with Fitted Parameters - All Materials

The following results in Table 3 and Table 4 are obtained from the comparison between the measurement data in 1.2mm distance and the simulations in the same procedure as shown above.

Material	Geometry	Parameters	Fitted Parameters	Max. dist ₁	Max. dist ₂
neofer_25_60p	Cube	Br=400	Br=360, $\mu = 1.07$	1mT	0.5mT
neofer_25_60p	L-Shape	Br=400	Br=370, $\mu = 1.15$	0.9mT	0.9mT
neofer_40_100p	Cube	Br=460	Br=425, $\mu = 1.07$	0.3mT	0.2mT
neofer_40_100p	L-Shape	Br=460	Br=452, $\mu = 1.15$	1.1mT	0.8mT
neofer_48_60p	Cube	Br=540	Br=470, $\mu = 1.02$	1.7mT	0.4mT
neofer_48_60p	L-Shape	Br=540	no fitting parameter	---	---

Table 3: Results from comparison of measurement data with negative part and the simulations without the freezing condition. The goal was to fit the parameters of the simulation with the measurement. To compare the fitted parameters achieved from the comparison of simulation and measurement, \mathbf{B}_r from the data sheets of Magnetfabrik Bonn is given. Additionally, the maximum distance between the measurement data as well as the maximum distance between measurement data and the simulation with fitted parameters can be seen.

Material	Geometry	Fitted Parameters	Max. dist ₃	H_{freeze}
neofer_25_60p	Cube	Br=360, $\mu = 1.07$	0.2mT	3.5T
neofer_25_60p	L-Shape	Br=370, $\mu = 1.15$	0.5mT	3.7T
neofer_40_100p	Cube	Br=425, $\mu = 1.07$	0.2mT	3.8T
neofer_40_100p	L-Shape	Br=452, $\mu = 1.15$	0.5mT	3.7T
neofer_48_60p	Cube	Br=470, $\mu = 1.02$	0.1mT	3.7T
neofer_48_60p	L-Shape	no fitting parameter	---	---

Table 4: Continuation of Table 3. Results from comparison of measurement data without negative part and the simulations including the freezing condition. The goal was to find the freezing field that fits the measurement data best. In this table the maximum distance between measurement data and the simulations with the freezing field that fits best can be seen.

Max. dist₁ is the maximal distance between the z-component of the measurement with the negative part and the measurement without the negative part.

Max. dist₂ describes the maximal distance of the z-component of the simulation without the freezing condition in comparison to the z-component measurement data without the negative part.

Max. dist₃ indicates the maximal error of the z-component of the simulation with the freezing condition in comparison to the measurement data without the negative part.

In nearly all of the cases the data of the measurement had to be shifted in the horizontal direction to be fitted. For the materials neofer_25_60p and neofer_40_100p the simulations with the fitted parameters coincide almost perfectly with the measurements. However, although a lot of simulations with different parameter

combinations were compared to the measurement data for neofer_48_100p, the best fit does not match the x-component exactly. However, the simulation that fits both components best simultaneously, is for the parameters $\mathbf{B}_r = 470\text{mT}$ and $\mu = 1.02$.

5.2.6 Non-reproducible Measurement Data

For the neofer_48_100p L-Shape, it is not possible to reproduce the measurement data with the simulation:

Comparing the shifted data of both measurements for the neofer_48_100p L-Shape shows a slightly different behavior as seen in Figure 32. Whereas for the other two materials, the measurement with the negative part has a higher magnetic field in the z-component than the measurement without the negative part, with neofer_48_60p it is conversely.

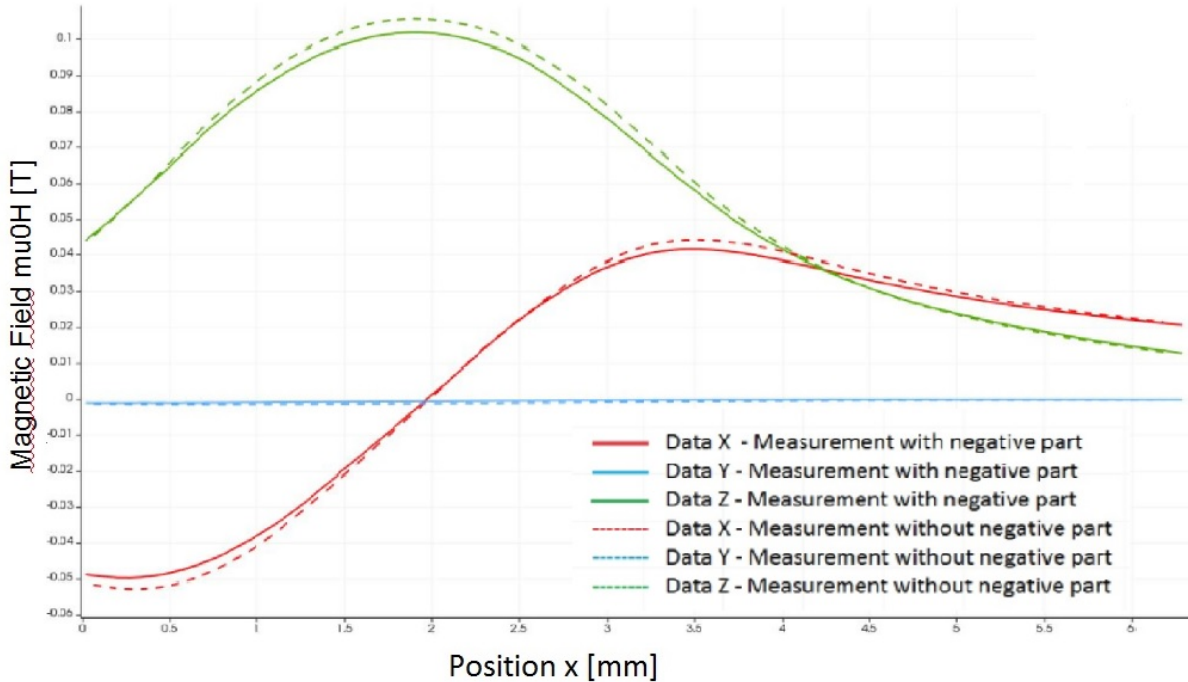


Figure 32: Comparison of measurement data neofer_48_60p. The data of this measurement are not reproducible by FEMME simulations.

This indicates an error in the measurement. If the freezing condition is considered in the simulation, the rotation of the final remanent magnetization is observed. This rotation in the magnetization, the flower state, implies that the magnetization in the z-direction is less than for the simulation without the freezing condition, since the magnetization vectors are not perfectly aligned in z-direction. The evaluation of the

measurement shows that it is likely that some error happened during the measurement. Thus, it is not possible to find a freezing field for the neofer_48_60p L-Shape.

5.2.7 Results - Data Sheet All Materials

The freezing fields achieved from the comparison of the measurement data and the simulations are higher than expected. The question arises how the fitting of the parameters \mathbf{B}_r and μ affects the resulting freezing field. Thus, another comparison between the measurement data without the negative part and simulations with the remanence from the data sheets from Magnetfabrik Bonn was done. The permeability is assumed to be $\mu = 1.15$.

Material	Geometry	Br	H_{freeze}
neofer_25_60p	Cube	Br=400	0.28T
neofer_25_60p	L-Shape	Br=400	0.2T
neofer_40_100p	Cube	Br=460	0.7T
neofer_40_100p	L-Shape	Br=460	1.2T
neofer_48_60p	Cube	Br=540	0.38T
neofer_48_60p	L-Shape	Br=540	no H_{freeze}

Table 5: Results from comparison of measurement data without negative part and the simulations including the freezing condition. The remanent magnetization \mathbf{B}_r is taken from the data sheets of Magnetfabrik Bonn.

The resulting freezing fields in this comparison are much lower than the freezing fields in the simulations with fitted parameters.

However, the accordance between measurement data and the freezing simulations is not as good as for the fitted parameters. This can be seen in Figure 33. As an example for the difference between the simulations with fitted \mathbf{B}_r and the simulations with the data from the data sheet, plots from the neofer_25_60p - cube are shown in Figure 34.

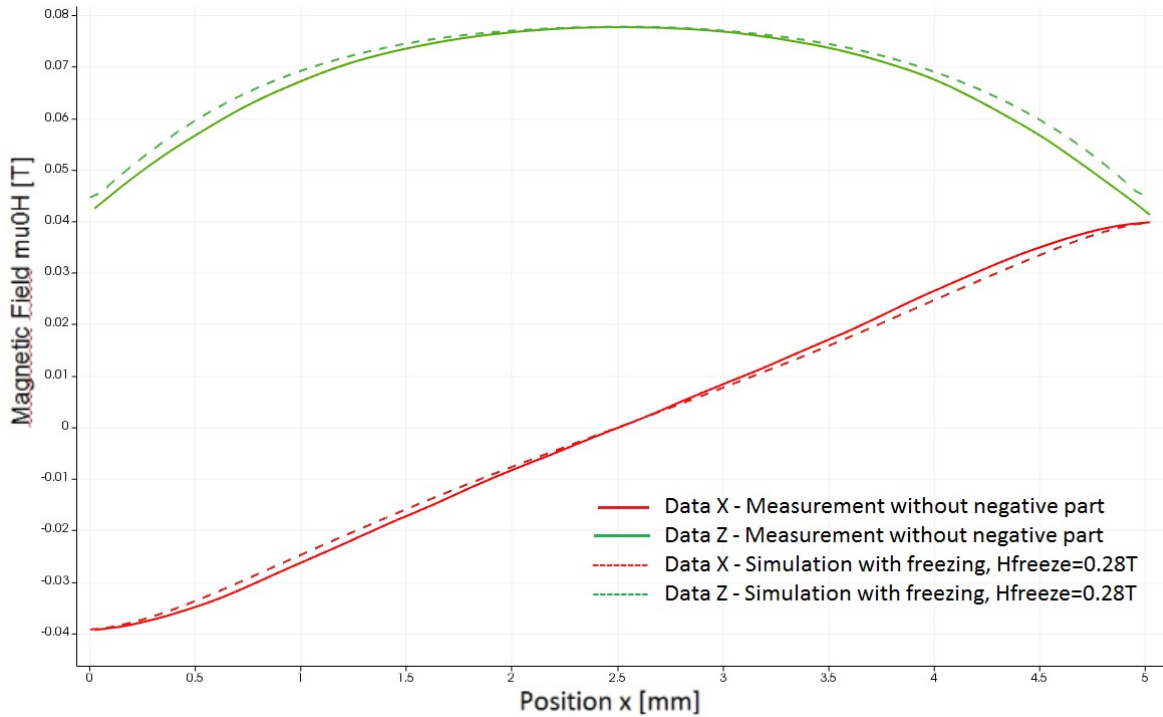


Figure 33: Comparison of measurement data without negative part and simulations of neofer_25_60p - cube with freezing effect and remanence from data sheet of MF Bonn.

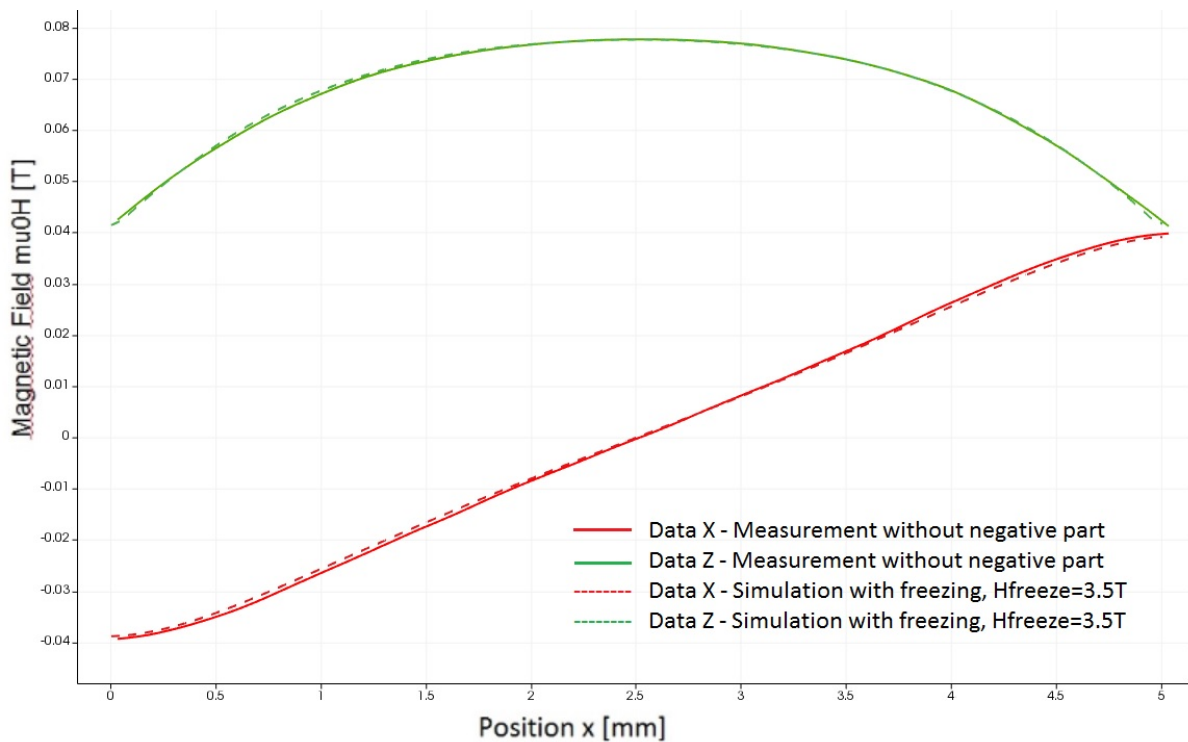


Figure 34: Comparison of measurement data without negative part and simulations of neofer_25_60p - cube with freezing effect, fitted remanence $B_r=360\text{mT}$ and fitted transversal susceptibility $\mu = 1.07$.

5.3 Conclusion

In this section, measurement data were compared with simulations of isotropic magnet including the freezing condition. The results should be improved further by switching the freezing field when \mathbf{B}_r and μ are correctly chosen. The comparison shows that the match between measurement and simulation is much better when \mathbf{B}_r and μ are fitted first. In this case the freezing field is approximately constant for all geometries and materials. The accordance between the measurement data and simulations without the freezing condition is nearly as good as the one when the freezing field is adjusted. Thus in this case, switching the freezing field does not really have influence on the results. When one does not fit the parameters but takes \mathbf{B}_r and χ from the data sheets, switching the freezing field improves the results. In this case, the freezing field is different for every material and every geometry. However, the match between measurement and simulations in this case is not as good as for the fitted parameters.

6 Discussion and Outlook

The aim of this work was to analyze a simpler vectorial hysteresis model, the freezing model, for the simulations of isotropic magnets and to determine the freezing field H_{freeze} . Interesting results have been achieved from the analysis of the model and new questions arose within the work.

The main effort of this work were the comparison of the freezing model with models of a magnet with uniaxial anisotropy, the computer experiment to determine H_{freeze} theoretically and the comparison between the FEMME simulations of isotropic magnets with real measurements. In this section, the main results will be summarized and further questions related to the freezing model will be presented.

6.1 Main Results

Comparisons of FEMME simulations of an isotropic magnet including the freezing condition and FEMME simulations of a magnet with anisotropic material law showed that these simulations differ from each other. (see Section 3) The parameters in the simulations, i.e., the freezing field H_{freeze} for the freezing simulation and the transversal susceptibility for the anisotropy simulation were chosen in order to get the same average magnetization in one component. Then, the average magnetization of the other components was checked. Since it is not possible to choose the parameters such that the average magnetization in all three components matches, the conclusion was that the freezing model cannot be described with an anisotropy model.

The results of the computer experiment (see Section 4) to determine the freezing field H_{freeze} based on a Stoner - Wohlfarth model showed a different behavior than expected. The obtained freezing fields for a rotation about 90° and 180° are higher than expected from a previous comparison of measurement data with simulations. Additionally, the freezing field seems to be dependent on the size of the rotation, which can be seen from the received results. Although a Stoner - Wohlfarth model is a good approximation to real-world magnetic material, the ratio between H_k and H_c is not correct and yields too high coercivities for different material parameters. Thus, the correct ratio between H_k and H_{ci} was gained by hysteresis matching.

Last but not least the comparison of measurement data received from Magnetfabrik Bonn with FEMME simulations were done (see Section 5). The goal was to find the freezing field H_{freeze} for two different geometries and three different materials. It has been shown that the obtained freezing fields are heavily dependent on the way the comparison was done. In one method the first step of the comparison was to fit the

remanence magnetization B_r and the transversal susceptibility μ in the simulation without the freezing condition. The achieved freezing fields in this case are then nearly constant about 3.7T for all geometries and all materials.

The second method of comparison was to take the remanence magnetization from the data sheets of Magnetfabrik Bonn and to assume the transversal susceptibility to be 0.15 in all cases. The resulting freezing fields are then much lower than the ones in the first method and they also vary between different materials and the two geometries. However, in this comparison the deviation between the simulations and the real measurement data is much bigger than for the first method, where B_r and μ are fitted.

6.2 Future Development

The comparison between the freezing model and a magnetic anisotropy model showed that the freezing effect cannot be described by an anisotropic susceptibility model. However, discussions with Magnetfabrik Bonn revealed that it might be possible to express "freezing-like" behavior with certain concepts of anisotropy. Thus, further work on this topic in cooperation with Magnetfabrik Bonn is suggested to get a deeper insight in this scope.

The computer experiment was performed with magnum.fd which is based on a finite-difference approximation. As already mentioned, a simple Stoner - Wohlfarth model assumes $H_k = H_c$ which leads to too high coercivity fields H_{ci} . With magnum.fd, the ratio between H_k and H_c cannot be adjusted. The correct ratio between H_k and H_{ci} has been obtained with the help of an extended SW model, where the component of the applied field within the easy axis direction is scaled.

It was attempted to repeat the computer experiment with the devicemodel and the correct ratio between H_k and H_{ci} . Unfortunately, the devicemodel only works in 2D, so currently it is not possible to correctly simulate the computer experiment with it. However, if this is fixed and 3D simulations can be performed with the devicemodel, the computer experiment will be repeated with the correct ratio between H_k and H_{ci} .

Different methods of comparing the FEMME simulations of isotropic magnets with measurement data from Magnetfabrik Bonn showed different behavior of the obtained freezing fields. The freezing fields obtained from the comparison with the remanence magnetizations taken from the data sheets were closer to the expected freezing fields. However, also the transversal susceptibility has to be taken into account, which is different for different materials. When comparing the measurement data with simulations, where different transversal susceptibilities are considered, other freezing fields are obtained. Hence, the freezing field seems to be heavily dependent on the

choice of the remanence magnetization B_r and the transversal susceptibility χ_t in the simulations. Pursuing comparisons between measurement data of other geometries and different materials would be helpful to see the behavior of the freezing field better, also regarding the fact that the cube and the L-shape are very simple and also similar geometries. This further work could also show whether the freezing field will stay a fitting parameter or not.

References

- [1] F. Bruckner, C. Vogler, M. Feischl, D. Praetorius, B. Bergmair, T. Huber, M. Fuger, and D. Suess. "*3D FEM–BEM-coupling method to solve magnetostatic Maxwell equations.*" *Journal of Magnetism and Magnetic Materials* 324.10 (2012): 1862-1866.
- [2] F. Bruckner, C. Abert, C. Vogler, F. Heinrichs, A. Satz, U. Ausserlechner, G. Binder, H. Koeck, and D. Suess. "*Macroscopic Simulation of Isotropic Permanent Magnets.*" *Journal of Magnetism and Magnetic Materials* 401 (2016): 875-879.
- [3] C. S. Koh, S.-y. Hahn, and G.-S. Park. "*Vector hysteresis modeling by combining Stoner-Wohlfarth and Preisach models.*" *IEEE transactions on magnetics* 36.4 (2000): 1254-1257.
- [4] A. Stancu, and C. Papusoi. "*Vector Hysteresis Modeling.*"
- [5] C-G. Stefanita. "*Magnetism: basics and applications.*" Springer Science & Business Media, 2012., ISBN: 978-3-642-22976-3
- [6] H.D. Young, and R.A. Freedman. "*University Physics.*" Sears and Zemansky's, 2008., 12th Edition, ISBN: 978-0-321-50130-1
- [7] G. Bertotti, and I. Mayergoyz. "*The Science of Hysteresis.*" Volume I., Academic Press, 2006., ISBN: 978-0-12-369431-7
- [8] Hilda WF Sung, and Czeslaw Rudowicz. "*A closer look at the hysteresis loop for ferromagnets-A survey of misconceptions and misinterpretations in textbooks.*" arXiv preprint cond-mat/0210657 (2002).
- [9] Fish, Gordon E. "*Soft magnetic materials.*" *Proceedings of the IEEE* 78.6 (1990): 947-972.
- [10] B. D. Cullity, and C. D. Graham. "*Introduction to Magnetic Materials.*" Wiley, 2009., ISBN: 978-0-470386323
- [11] J.D. Jackson. "*Classical Electrodynamics.*" Wiley, 1998., Third Edition, ISBN: 978-0-471309321
- [12] I. Mayergoyz, M. Chari, and J. D'angelo. "*A new scalar potential formulation for three-dimensional magnetostatic problems.*" *IEEE transactions on magnetics* 23.6 (1987): 3889-3894.

- [13] O. Biro, K. Preis, G. Vrisk, and K.R. Richter. "*Computation of 3-D magnetostatic fields using a reduced scalar potential.*" IEEE Transactions on Magnetics 29.2 (1993): 1329-1332.
- [14] A. C. Hindmarsh, P. N. Brown, K. E. Grant, S. L. Lee, R. Serban, D. E. Shumaker, and C. S. Woodward. "*SUNDIALS: Suite of Nonlinear and Differential/Algebraic Equation Solvers.*" ACM Transactions on Mathematical Software, 31(3), pp. 363-396, 2005. Also available as LLNL technical report UCRL-JP-200037.
- [15] O. Chadebec, J-L. Coulomb, and F. Janet. "*A review of magnetostatic moment method.*" IEEE transactions on magnetics 42.4 (2006): 515-520.
- [16] E. Della Torre. "*A simplified vector Preisach model.*" IEEE transactions on magnetics 34.2 (1998): 495-501.
- [17] I. Mayergoyz. "*Mathematical models of hysteresis.*" IEEE Transactions on magnetics 22.5 (1986): 603-608.
- [18] I. D. Mayergoyz. "*Mathematical Models of Hysteresis and Their Applications.*" Elsevier, 2003., ISBN: 978-0-12-480873-7
- [19] E. Della Torre, and L. H. Bennett. "*Analysis and simulations of magnetic materials.*" DYNAMICAL SYSTEMS 2005 (2005): 854-861.
- [20] E. C. Stoner, and E. P. Wohlfarth. "*A mechanism of magnetic hysteresis in heterogeneous alloys.*" Philosophical Transactions of the Royal Society of London A: Mathematical, Physical and Engineering Sciences 240.826 (1948): 599-642.
- [21] D.L. Aherton, and J. R. Beattie. "*A mean field Stoner-Wohlfarth hysteresis model.*" IEEE transactions on magnetics 26.6 (1990): 3059-3063.
- [22] G. Bertotti. "*Hysteresis in magnetism: for physicists, materials scientists, and engineers.*" Academic press, 1998.
- [23] R. Wood. "*Exact solution for a Stoner–Wohlfarth particle in an applied field and a new approximation for the energy barrier.*" IEEE Transactions on Magnetics 45.1 (2009): 100-103.
- [24] F. Bruckner, B. Bergmair, H. Brueckl, P. Palmesi, A. Buder, A. Satz, and D. Suess. "*A device model framework for magnetoresistive sensors based on the Stoner–Wohlfarth model.*" Journal of Magnetism and Magnetic Materials 381 (2015): 344-349.

- [25] D. C. Jiles, and D. L. Atherton. *"Theory of ferromagnetic hysteresis."* Journal of magnetism and magnetic materials 61.1-2 (1986): 48-60.
- [26] J.Wang, H. Sepehri-Amin, Y.K. Takahashi, S. Okamoto, S. Kasai, J.Y. Kim, T. Schrefl, and K. Hono. *"Magnetization reversal of FePt based exchange coupled composite media."* Acta Materialia 111 (2016): 47-55.
- [27] R. Skomski. *"Simple Models of Magnetism."* Oxford Graduate Texts, 2008., ISBN: 978-0-19-857075-2
- [28] A. K. Patra. *"Crystal Structure, Anisotropy and Spin Reorientation Transition of Highly Coercive, Epitaxial Pr-Co Films."* Cuvillier Verlag, 2008., ISBN: 978-3-867277730
- [29] U. Hartmann. *"Origin of Brown's coercive paradox in perfect ferromagnetic crystals."* Physical Review B 36.4 (1987): 2331.
- [30] C. Abert, G. Selke, B. Krüger, and A. Drews. *"A fast finite-difference method for micromagnetics using the magnetic scalar potential."* IEEE Transactions on Magnetism 48.3 (2012): 1105-1109.
- [31] Pietro Palmesi. *"Thermal Description of GMR Sensors Using Monte-Carlo Simulations Based on the Stoner-Wohlfarth Model."* Diploma Thesis. TU Wien. 2014